A STUDY OF DETACHED SHOCK WAVES IN TWO-DIMENSIONS

Thesis by

Morton Alperin

In Partial Fulfillment of the Requirements

For the Degree of

Doctor of Philosophy

California Institute of Technology

Pasadena, California

1950

ACKNOWLEDGMENT

The author wishes to take this opportunity to express his appreciation to the many people who participated in the various phases of the work involved in this investigation. In particular he wishes to mention Dr.'s H.J. Stewart and H.T. Nagamatsu of the California Institute of Technology, with whom the author had many valuable discussions regarding the experimental phases of the work as well as the theoretical. Mr. Harry Barnett of the Jet Propulsion Laboratory has been of invaluable assistance in handling many design problems connected with the two-dimensional wind tunnel and the experiments performed in it.

It has also been the privilege of the author to have spent many hours with Dr. Th. von Kármán who suggested the method of treatment of the detached shock wave problem outlined in section IV of this thesis. During these meetings, the general problem as well as the details of special examples were discussed and it is hoped that some of these examples will be the subject of future papers. The author is deeply grateful to Dr. von Kármán and wishes to take this opportunity to express his appreciation.

The author is indebted to the Army Ordinance Department for their support of the experimental program, also to Miss Mary Schulte for her work in preparing the final draft of this thesis.

ABSTRACT

The present report contains results of an experimental and theoretical investigation of the detached shock wave phenomenon. The experimental phase of this study was actually carried out at the Jet Propulsion Laboratory at California Institute of Technology, in a two-dimensional wind tunnel which is briefly described in Section I.

Section II contains a description of the experiments on circular cylinders. The circular cylinder was used in this series of tests primarily because of its simplicity. The investigation discussed in II-1 required a large variation of model shapes and would have required much more time had it been based on a more complicated body shape. In addition to data on the shock wave position and shape, the pressure distribution was also obtained at $M = 1.546$ for a two-dimensional circular cylinder. From this pressure distribution, the drag was calculated.

Although the theoretical knowledge of flow involving detached shock waves is in a rather primitive state, a review of the existing theoretical work and comparison with experimental data is made in section III.

In section IV a method is presented for finding the stream function or velocity potential for the subsonic region behind the detached shock wave. This method depends upon the hypothesis that the flow can be considered to be irrotational in this region without introducing a serious error. The results appear to be in good agreement with the experiments although the example carried out does not apply strictly to the circular cylinder body shape used in the experiments.

A general discussion of the existing theories and their comparison with experimental data is presented in section V.

CONTENTS

INTRODUCTION

During the past few years, there has been considerable interest in the theoretical treatment of the detached shock wave phenomenon. Papers have been presented by several authors (references 3,4,5,6) and a variety of results appeared which did not agree with each other as closely as could be desired. Thus the need for experimental data to serve as a basis for comparison was obvious and the Jet Propulsion Laboratory of California Institute of Technology undertook this work.

A two-dimensional tunnel 5" x 28" in cross section was designed especially for this purpose. Some details of this tunnel are described briefly in section I of this paper.

The experimental program was initiated with the purpose of obtaining experimental data on two-dimensional flow and therefore the first phase was concerned with the problem of estimation of the end effects. It was found that even independent of boundary layer-shock wave interaction effects, a circular cylinder of span/diameter ratio of 30 was required to obtain essentially uniform conditions across a major portion of the span. The interaction of the tunnel wall boundary layer with the shock wave made it necessary to increase the span/diameter ratio to 50 to obtain a uniform field in the spanwise direction. More details concerning this phenomenon are contained in section II of the present paper.

In addition to the information regarding shock wave position and shape for a two-dimensional circular dylinder, the pressure distribution around the surface of such a cylinder in two-dimensional flow was also obtained and is discussed in section II-2.

All this work was done at $M = 1.546$ since the two-dimensional tun-

nel had only one fixed nozzle at the time of these experiments. Similar data, however, were obtained in the 12" supersonic tunnel at J.P.L. and are presented in this paper for a range of Mach Numbers between 1.35 and 2.0.

As far as could be done these experimental data are compared with various theories in section III. The comparison shows most of the theoretical work to be in disagreement with the experimental data. Some of the reasons for this discrepancy are pointed out in the discussion of section VI.

In conjunction with the experimental program a theoretical investigation of the phenomenon was also carried out. A method originally suggested by Dr. Th. von Kármán was applied to the flow about a circular cylinder. The general method is presented in section IV and the special case of the flow about a circular cylinder is carried out in detail in section V.

The method consists of an application of the so-called Kármán-Tsien procedure which implicitly involves the assumption of irrotational flow behind the shock wave, and the existence of the velocity potential as well as the stream function. The case of the circular cylinder was then carried out by assuming that the complex potential in the corresponding incompressible flow hodograph plane is of the same form as that for a circular cylinder; however a special technique had to be devised to satisfy the boundary condition behind the shock wave rather than at infinity as is usually done in subsonic problems.

This procedure gave a body shape in the compressible fluid physical plane which deviated from the circular cylinder by a factor proportional to the derivative of the incompressible velocity with respect to the compressible velocity $(\frac{dq}{dw})$. Comparison of this flow field with

that of a circular cylinder in the two-dimensional wind tunnel is shown on figures 13 and 14 and is discussed in more detail in section VI-5.

I. DESCRIPTION OF WIND TUNNEL

The wind tunnel used in the present investigation is a nonreturn tunnel having a 5" x 28" test section (Fig. 1). It had previously been designed for subsonic testing of inlet diffuser models and was redesigned to suit the needs of the detached shock wave investigation.

The tunnel is located in a ramjet test pit and consists of a steel inlet nozzle (subsonic), laval nozzle and a plywood diffuser. The air is supplied by the regular test pit blower facilities consisting of four blowers and a valving arrangement for series or parallel operation. The air is also dried before entering the tunnel.

1. Power Plant

The air supply for operation of the wind tunnel comes from a central power plant consisting of four electrically driven centrifugal compressors. Two of these are rated at 8000 cfm and 2.06 compression ratio, the other two at 14,000 cfm and 2.1 compression ratio. The piping and valves are arranged so that these compressors can be run in parallel or series-parallel; the performance of each combination is shown on Fig. 2.

2. Test Section

A portion of the subsonic nozzle, the supersonic nozzle, and test section are contained in the heavy steel plates adapted from the subsonic tunnel (Fig. 1). The supersonic nozzle is of the fixed type; the curved surfaces are wood spacer blocks 5 inches wide and 28 inches apart at the test section.

Only 9 inches of this 28 inches are available for schlieren pictures since this was the window size already incorporated in the side walls of the subsonic tunnel. The 28 inch height is essential to avoid choking or interference of reflected shock waves, phenomena which generally determine the limits of usefulness of a supersonic wind tunnel.

More detail relative to the actual design procedure used in obtaining the shape of the supersonic nozzle blocks will be given later.

One steel side wall is rigidly fixed to the plenum chamber and inlet contraction duct, the other is mounted on rollers for ease in handling during changes of the fixed wooden nozzles. These nozzles are positioned by means of steel inserts which are doweled into the side plates.

3. Diffuser

The diffuser simply consists of a plywood box tapered both horizontally and vertically. The external surfaces of the diffuser have been encased in soundproofing materials to reduce the noise level in the vicinity of the tunnel.

4. Schlieren System

The schlieren system is a conventional 2-mirror type having a G.E. BH-6 light source. The power supply to the light source is arranged so that the bulb can be operated continuously or in extremely short duration (5 micro seconds) flashes. Both types of operation have proved extremely useful in clarifying various phenomena which will be discussed later in this report.

5. Survey Mechanism

The tunnel is equipped with an electrically operated survey mechanism. This consists of a hollow rectangular bar which moves axially along the tunnel center line completely through the test section. The position of the bar is registered on a dial on the outside of the tunnel. There is also a smaller survey mechanism attached to the large shuttle which can be positioned accurately to any desired position in the test section. The smaller vernier control is also actuated from outside the tunnel and is used for extremely accurate settings of total head or static tubes.

6. Supersonic Nozzle Design

Since most of the initial work planned for the tunnel did not require changes in the Mach number, the tunnel was designed with fixed nozzle blocks which, however, were made easily interchangeable.

The nozzle blocks consisted simply of an upper and lower wooden spacer separating the steel side walls and having the proper shape on the inner surface in contact with the air flow.

The calculation of this inner shape to obtain uniform supersonic flow at a given Mach number was the major problem in the entire design; therefore a brief discussion of this calculation will be presented here.

The streamline shape required to obtain a uniform flow at a given Mach number greater than 1.0, in a nonviscous fluid, can be determined either graphically, by the method of characteristics, or analytically by a method presented in Ref. 1. The analytical method was used in the present design.

Since in a real fluid the boundary layer changes both the streamline shape and the effective cross-sectional area of the duct, a correction must be applied to the results of the perfect fluid theory to account for this effect, if uniform flow is to be expected.

The actual streamline shape in the vicinity of the wall cannot be determined, but corrections to the shape based on a boundary layer displacement thickness calculated as discussed in Ref. 2 can be made. This method, although theoretically crude, produced very uniform flow in the test section. The method was applied in the following manner. The boundary layer thickness, δ, was determined as a function of the distance from the throat. The value of $\frac{\partial \delta}{\partial x}$ in the test section was known from experimental data taken in the twelve-inch tunnel at the Jet Propulsion Laboratory. The boundary layer thickness as calculated by the

method of Ref. 2 was then modified to produce the proper wall slopes at the test section. It then remained to correct the basic shape obtained by the analytical method of Ref. 1 by an amount ΔY determined as follows. Using the notation of Fig. 3

$$(Y + \Delta Y)2\delta + b\delta = \Delta Y (b - 2\delta)$$

$$\Delta Y = \frac{\delta(2Y/b + 1)}{1 - 4Y/b}$$

where

δ - displacement thickness (corrected by experimental data in twelve-inch tunnel)

Y - ordinate calculated from nonviscous theory as a function of x for a given Mach number.

The final shape is given as

$$X = X(Y + \Delta Y)$$

The flow in the test section was surveyed with a total head tube and with a wedge of semi-angle $\delta = 4.13°$. The results of these surveys were in very close agreement and therefore only the wedge data are shown in Fig. 4. The deviations of the flow are extremely small and any existing wave pattern is so weak that it cannot be seen with the schlieren equipment.

II. DESCRIPTION OF EXPERIMENTS

The primary objective of this investigation was to obtain data on two-dimensional flow with detached shock waves. The data would be useful as a criterion of the accuracy of the assumptions of any given theory.

1. Tunnel Wall Effect

The first phase of the experimental program consisted of a determination of the model dimensions needed to obtain two-dimensional flow. Because of the fact that the region behind the shock wave is partially subsonic, and the remainder is supersonic, it is impossible to predict to what extent the boundary conditions (i.e. tip conditions) affect the entire flow field. The presence of a boundary layer on the side walls of the tunnel adds still more uncertainty to the validity of the experimental results, since this boundary layer interacts with the shock wave and causes difficulty in interpretation of schlieren pictures, as well as actually causing a departure from two-dimensional flow over the entire subsonic field.

If, for example, a rod of uniform cross-section completely spans the tunnel as shown in Fig. 5, the schlieren picture taken from the side as in Fig. 5b does not show the true two-dimensional shock wave shape and position with respect to the body. Actually the schlieren picture in this case shows an extremely thick compression region due to the end effect and the location of the shock wave cannot be determined from such a picture.

The tunnel used in this investigation was not equipped with a schlieren system capable of taking pictures corresponding to Fig. 5a, and therefore it was not certain whether or not the shock wave-boundary layer interaction at points A and B affected the entire shock wave between A and B. Thus before any conclusions could be made this difficulty had to

be overcome. The most obvious method of minimizing this difficulty was to reduce the span of the model. This was done and the resulting configuration is shown in Fig. 6.

Reduction of the model span, so that the ends did not protrude into the boundary layer, resulted in clearer schlieren pictures (Fig. 6b). The schlieren photograph of the shock is much more distinct than that for a full span model (Fig. 5b), but evidently the difficulty is not entirely overcome since on Fig. 6b there still appears to be some peculiar three-dimensional effect. The shock wave still extended beyond the model tip in the spanwise direction and intersected the boundary layer as shown in Fig. 6a, thus causing peculiarities in the resulting photograph. The question as to what model dimensions would produce a uniform two-dimensional shock wave which could be photographed clearly enough for the necessary data to be measured still had no satisfactory answer.

By rotating the model 90° about the tunnel axis and taking pictures of cylinders with various span/diameter ratios it was found that uniform two-dimensional flow could be obtained only with span/diameter ratios exceeding 30. Testing models in this position (Fig. 7) did not give the shock wave shape but did show its uniformity in the spanwise direction. The results of these tests are shown as X's on Fig. 8. In this vertical position the shock wave-boundary layer interaction was minimized since the wave curved backward sufficiently to obtain a supersonic flow barrier (Fig. 9) between the model and the boundary layer.

Since the principal interest lies in investigating the flow field behind the shock wave it is essential to test models in the horizontal position as in Figs. 5 and 6, where this field is not obscured by the shock wave. Therefore it was necessary to determine if models of span/diameter ratios as low as 30 would still produce two-dimensional flow

when tested in this position. The results of testing approximately 50 models and taking over 200 schlieren pictures are summed up in Fig. 8. The models had various spans varying from 2 inches to 5 inches and diameters varying from 1/16" to 3/4".

It is clear from Fig. 8 that span/diameter ratios (b/d) of approximately 50 should be used to avoid the effect of the boundary layer-shock wave interaction. The effect of varying model span (b) in relation to tunnel width (w) is also shown on Fig. 8. For large enough values of b/d the value of b/w does not matter except for clarity of photographs. From this point of view values of $b/w < 0.8$ were required in this particular wind tunnel.

Fig. 10 is a schlieren photograph of a 1/16" diameter model having a span of 3 inches. This is included as a picture which represents true two-dimensional flow past a circular cylinder at $M = 1.546$. Unfortunately it was necessary to use extremely small models (1/16" diameter) to attain two-dimensional flow but the data were very carefully measured by enlargement of photographs taken on glass plates. The analysis of this picture gives the following data

$$L/R = 2.72$$

$$L/R_s = 0.1875$$

where

L - detachment distance

R - cylinder radius

R_s - radius of curvature of shock wave

for

$$M = 1.546$$

$$R.N. = \frac{2 \rho_\infty U_\infty R}{\mu} = 79.5 \times 10^3$$

Since the two-dimensional tunnel in which these experiments were

performed had fixed nozzles, data were obtained at a range of Mach numbers between 1.3 and 2.0 in the 12" wind tunnel at the Jet Propulsion Laboratory. The model used for this purpose was 1/4" in diameter and 10" in span. These data are presented in Figs. 13 and 14 and are in excellent agreement with the data obtained in the 5" x 28" two-dimensional tunnel.

2. Pressure Distribution Around Circular Cylinder

In order to measure the pressure distribution around the surface of a circular cylinder, a hollow rod 3/16" in diameter, having a pressure orifice midway between its ends was mounted vertically in the tunnel, protruding at the top and bottom. The span was therefore equal to the effective tunnel height (approximately 28"). The tube was supported at both ends by thrust bearings and put under tension to avoid excess bending. Provision was made to rotate the tube about its longitudinal axis so that the pressure on the hole drilled in its surface could be read at different angular positions. Fig. 11 is a plot of this pressure, in terms of the stagnation pressure, versus angular position around the cylinder. Fig. 12 is a schlieren picture of the tube showing the two-dimensional character of the flow past the cylinder.

The drag coefficient per unit length of cylinder was calculated from the pressure distribution shown on Fig. 11. It was defined as follows

$$C_D = \frac{1}{\gamma p M^2} \int p' \cos\theta \, d\theta$$

p' - pressure on cylinder surface

p - free stream static pressure

The integral was evaluated graphically and gave a value of

$$C_D = 1.447 \text{ for } M = 1.546$$

Further experiments are planned to obtain similar data over a range

of Mach numbers but have not been completed as yet. It is of interest, however, to compare these data with some existing theories.

III. DISCUSSION OF SEVERAL THEORIES AND COMPARISON WITH EXPERIMENT

Since several theories describing the detached shock flow regime have recently been published and since there are apparently very few two-dimensional data available for comparison, a brief review of each of these theories and comparison with the previously discussed experimental data will be given here.

1. Nagamatsu's Theory

One of the first and simplest theories on the subject of detached shock waves was presented by Henry T. Nagamatsu in his doctorate thesis, Ref. 3. In this theory Nagamatsu has attempted to calculate the shock wave detachment distance for several differently shaped bodies, both two-dimensional and axially symmetric. The method used was as follows.

The flow downstream of the detached wave was assumed to have a velocity distribution equivalent to that of the same body in an infinitely extended incompressible flow, corrected for the effects of compressibility by the Prandtl-Glauert rule. Then, by matching the velocity on the axis with that behind a normal shock wave at a given free stream Mach number, the position of the wave was fixed for the given value of M. To be more specific, the case of a two-dimensional circular cylinder will be worked out in detail.

It is well known that the flow of an incompressible fluid past such a cylinder is given by the potential function for the perturbation velocities

$$F = \frac{Ua^2}{z}$$

where

a - radius of the cylinder

U - velocity of flow at infinity

The velocity field is then given by

$$F' = u - iv = -U\frac{a^2}{z^2}$$

and if we apply the Prandtl-Glauert factor to this we get

$$F' = \frac{-U}{\sqrt{1-M_2^2}}\left(\frac{a^2}{z^2}\right) \tag{1}$$

where M_2 is the Mach number behind a normal shock wave.

If a normal shock wave exists in a supersonic flow of Mach number M_1 then it is known from shock wave theory that

$$u = \frac{2}{\gamma+1}\left(\frac{M_1^2-1}{M_1^2}\right)U \tag{2}$$

where u is the change in velocity produced by the shock wave. Equating this to the real part of Eq. (1) on the x-axis gives

$$\frac{U}{\sqrt{1-M^2}}\left(\frac{a^2}{x^2}\right) = \left(\frac{2}{\gamma+1}\right)\left(\frac{M_1^2-1}{M_1^2}\right)U$$

or, solving for x/a gives

$$\frac{x}{a} = (1-M^2)^{\frac{1}{4}}\sqrt{\left(\frac{\gamma+1}{2}\right)\left(\frac{M_1^2}{M_1^2-1}\right)} \tag{3}$$

In this equation x is the distance from the origin to the shock wave.

Fig. 13 is a plot of the detachment distance $\left(\frac{x-a}{a} = \frac{L}{a}\right)$ vs free stream Mach number as determined by this theory. The experimental data obtained in the JPL tunnel **are** also plotted in this figure.

The detachment distance can be computed in this manner for many bodies whose incompressible solutions are known, but the theory has several obvious weaknesses, which account for the large discrepancy between experiment and theory. For example, by choosing a velocity distribution along the axis, the distance L is fixed. The body corresponding to this velocity distribution in a compressible fluid would probably be very different from that for an incompressible fluid, whereas this theory ne-

glects the change in body shape. A more exact calculation was carried out by Lin and Shen (Ref. 5) and although the method used is very elegant, the use of power series has proved to be very cumbersome.

2. Method of Lin, Shen and Rubinov

This method consists essentially of a power series solution of the equations for the adiabatic flow of a nonviscous, compressible fluid; valid in a region close to the shock nose point, and a matching of this solution with another series solution valid near the body nose. The method was first suggested in Ref. 4 by Lin and Rubinov in a slightly different form and will be discussed in some detail here.

The fundamental equations governing the flow are, in standard form

Continuity equation $$\nabla \cdot (\rho \bar{q}) = 0 \tag{4}$$

Equation of motion $$(\bar{q} \cdot \nabla)\bar{q} = -\frac{\nabla p}{\rho} \tag{5}$$

Adiabatic equation $$\frac{p}{\rho^{\gamma}} = F(\psi) = e^{\frac{S}{C_v}} \tag{6}$$

Equation of state $$\frac{p}{\rho} = RT \tag{7}$$

Conservation of energy $$JE_i + \frac{p}{\rho} + \frac{1}{2}q^2 = \frac{p}{\rho}\frac{\gamma}{\gamma-1} + \frac{1}{2}q^2 = \text{const.} \tag{8}$$

Since

$$(\bar{q} \cdot \nabla)\bar{q} = \frac{\nabla q^2}{2} + (\nabla \times \bar{q} \times \bar{q})$$

Eq. (5) may be written as

$$(\nabla \times \bar{q}) \times \bar{q} = -\frac{\nabla p}{\rho} - \frac{\nabla q^2}{2} \tag{9}$$

Now to obtain an equation involving only velocities the term $\frac{\nabla p}{\rho}$ must be eliminated from Eq. (9). This quantity can be expressed in terms of the velocity (q) and V_m, the maximum velocity obtainable by adiabatic expansion, as follows.

From equations (6) and (8)

$$\frac{\gamma}{\gamma-1} F(\psi) \rho^{\gamma-1} = \frac{V_m^2 - q^2}{2}$$

and therefore

$$\rho = \left[\frac{\gamma - 1}{2\gamma} \frac{V_m^2}{F(\psi)} \left(1 - \frac{q^2}{V_m^2} \right) \right]^{\frac{\gamma}{\gamma - 1}} \tag{10}$$

and using this in Eq. (6)

$$p = F(\psi)^{-\frac{1}{\gamma - 1}} \left[\frac{\gamma - 1}{2\gamma} V_m^2 \left(1 - \frac{q^2}{V_m^2} \right) \right]^{\frac{\gamma}{\gamma - 1}} \tag{11}$$

Taking the gradient of p and dividing by ρ gives

$$-\frac{\nabla p}{\rho} = \frac{1}{2\gamma} \left(V_m^2 - q^2 \right) \frac{d \ln F(\psi)}{d \psi} \nabla \psi + \frac{\nabla q^2}{2} \tag{12}$$

This is the expression for $\frac{\nabla p}{\rho}$ in terms of velocities. Substituting it into Eq. (9) gives

$$(\nabla \times \bar{q}) \times \bar{q} = \frac{1}{2\gamma} \left(V_m^2 - q^2 \right) \frac{d \ln F(\psi)}{d \psi} \nabla \psi$$

or

$$(\nabla \times \bar{q}) \times \bar{q} = \frac{1}{2\gamma} \left(V_m^2 - q^2 \right) \nabla \ln F(\psi) \tag{13}$$

The conventional stream function for axially symmetric flow is defined as follows. If we write Eq. (4) for the case under consideration it takes the form

$$\frac{\partial}{\partial z} (\rho u) + \frac{1}{r} \frac{\partial}{\partial r} (r \rho v) = 0 \tag{14}$$

Now we define a function ψ which satisfies Eq. (14) as

$$\begin{aligned} r \rho u &= \psi_r \\ r \rho v &= -\psi_z \end{aligned} \tag{15}$$

This defines the stream function in the conventional manner.

Rewriting Eq. (13) in cylindrical coordinates and assuming axial symmetry gives

$$\left(\frac{\partial v}{\partial z} - \frac{\partial u}{\partial r}\right) u = \frac{1}{\gamma - 1} \frac{p}{\rho} \frac{\partial}{\partial r}\left[F(\psi)\right]\left(\frac{1}{F(\psi)}\right)$$

$$-\left(\frac{\partial v}{\partial z} - \frac{\partial u}{\partial r}\right) v = \frac{1}{\gamma - 1} \frac{p}{\rho} \frac{\partial}{\partial z}\left[F(\psi)\right]\left(\frac{1}{F(\psi)}\right)$$

or in terms of ψ , both equations become

$$\frac{\partial}{\partial z}\left(\frac{1}{r\rho}\psi_z\right) + \frac{\partial}{\partial r}\left(\frac{1}{r\rho}\psi_r\right) = -\frac{r\rho^{\gamma}}{\gamma - 1} F'(\psi) \tag{16}$$

Equation (16) is known as the vorticity distribution equation and is a basic equation for the type of flow under consideration. Another equation is needed since there are two dependent variables, ψ and ρ in Eq. (16). The second equation is easily obtained by substitution of ψ and Eq. (6) into Eq. (8)

$$\frac{1}{2r^2\rho^2}\left(\psi_z^2 + \psi_r^2\right) + \frac{\gamma}{\gamma - 1} F(\psi)\rho^{\gamma - 1} = \text{const.} \tag{17}$$

Thus the problem consists of finding solutions of equations (16) and (17) which satisfy the particular boundary conditions. In this case we are interested in obtaining information in the region between the shock wave and the body, and a solution was obtained by Lin and Shen as follows.

Formally assume ψ and ρ to be of the form

$$\begin{aligned} \psi &= \psi_1(z) r^2 + \psi_2(z) r^4 + \dots \\ \rho &= \rho_0(z) + \rho_1(z) r^2 + \rho_2(z) r^4 + \dots \end{aligned} \tag{18}$$

the odd powers being omitted since the solution is desired for the symmetric flow only and therefore the coefficients of odd powers of r must be zero.

Inserting (18) into (16) and (17) and comparing powers of r gives

two series of differential equations for the coefficients of ψ and ρ respectively. Upon manipulation of these sets of equations the coefficients of the series can all be expressed in terms of ρ_0 and its derivatives.

Thus for any given choice of $\rho_0(z)$ the functions ψ and ρ can be approximately determined.

From the form of the assumed series (18) it is evident that the entire procedure is valid only in the neighborhood of the z-axis.

The extent of this neighborhood cannot be discussed from the series themselves since the general or n^{th} term is unknown. However, from the theory of power series in general it is known that these series converge within a circle whose radius is equal to the distance from the origin to the nearest singularity of the function. Thus for a proper choice of $\rho_0(z)$ the series should converge in a small region near the z-axis limited only by singularities within the body.

Further restrictions are placed on the region of convergence of the series by the method used to determine $\rho_0(z)$. This is done as follows.

The shock wave shape is assumed to be of the form

$$r^2 = \beta_1 z + \beta_2 z^2 + \beta_3 z^3 + \cdots \tag{19}$$

then the pressure, density and the function $F(\psi)$ immediately behind the shock are known in terms of the shock wave inclination α and can be expressed in terms of r^2 or z by the use of Eq. (19). $F(\psi)$ can then be expressed in terms of ψ from the relationship $\psi = \frac{1}{2}\rho_\infty U_\infty r^2$ for uniform axially symmetric flow. These expressions for ψ and ρ as functions of z with coefficients in terms of β's are then compared with power series obtained by inserting (19) into (18). Thus the coefficients are now determined in terms of the shock wave shape parameters (β_n).

The region of convergence has, however, been further restricted to the neighborhood of the shock wave nose by this procedure, since the coefficients have been evaluated at the shock wave itself.

The entire procedure is then repeated with the following difference. The expression for the shock wave shape is replaced by one for the body shape

$$r^2 = \epsilon_1 z + \epsilon_2 z^2 + \epsilon_3 z^3 + \ldots \tag{20}$$

and the conditions that furnish the relations for the determination of the coefficients are now those at the body nose instead of those immediately behind the shock. Thus another series solution in terms of the ϵ's can be found.

By matching the two solutions at the stagnation point, relationships involving β's, ϵ's and δ, the detachment distances are found and the β's and δ are expressed in terms of the body shape parameters.

The only examples carried out in detail by this method appear in Ref. 6. In this paper Dugundji carries out the calculation for the quantity L/R_s (detachment distance/radius of curvature of shock wave), for an axially symmetric body. The method used is that suggested by Lin and Rubinov (Ref. 4). For purposes of calculating L/R_s it is not necessary to use the expansion about the body nose and the Lin-Rubinov method is simpler; therefore, this method was used at the Jet Propulsion Laboratory to calculate the flow about a two-dimensional circular cylinder. Fig. 14 shows the results of this calculation and a comparison with experiment. The calculation included only two terms of the series, since in the axially symmetric case this seemed to give closer agreement with experiment than the calculation including the third term. The discrepancy in two-dimensional flow is much greater than that in the axially

symmetric flow discussed in Ref. 6. In fact, the same approximation as used in calculating the data for Fig. 14 gave excellent agreement in the axially symmetric case with experiments performed by Ladenburg (Ref. 7).

No definite conclusions can be drawn yet since there is a scarcity of experimental data, but it appears that the Lin method should be carried out to include more terms of the series if any useful information is to be expected.

3. Moeckel's Calculation

A very simplified procedure for calculation of the shock wave detachment distance and estimating the drag of the subsonic surfaces of the body is presented in Ref. (8).

The method consists essentially of assuming the shock wave to have a hyperbolic shape given by the equation

$$\beta y = \sqrt{x^2 - x_o^2}$$

where

β - the cotangent of the Mach angle

x_o - the distance from the vertex of the wave to the intersection of its asymptotes.

The sonic point on the body is assumed to be located at the point where the inclination of the surface is equal to the wedge or cone angle corresponding to shock detachment. The sonic point behind the shock is given by the shock wave shape.

The sonic line connecting these two points is assumed to be straight. The length of this straight sonic line is then determined by an approximate form of the continuity equation. The derivation of this equation and its use will be repeated here in order to show what approximations were made by Moeckel. For notation see Fig. 15.

The stagnation pressure immediately behind the shock wave is known

in terms of the free stream Mach number and the shock inclination. The approximate continuity equation is based on the use of an average value of this stagnation pressure. The average value is chosen as that value existing at the mass centroid of the fluid passing the sonic line. With this assumption the continuity equation can be written as follows.

$$\frac{A_o}{A_s} = \frac{(\rho_s v_s)_c}{\rho_o v_o} = \left(\frac{P_s}{P_o}\right)_c \frac{T_o}{T_s} \frac{v_{cr}}{v_o}$$

where the subscripts are defined as follows

o - free stream

s - sonic line

c - centroid of mass

cr - critical (M = 1) section

Since the stagnation temperature is constant across a shock wave

$$\frac{A_o}{A_s} = \left(\frac{P_s}{P_o}\right)_c \left[\frac{1 + \frac{\gamma-1}{2}}{1 + \frac{\gamma-1}{2}M^2}\right] \frac{v_{cr}}{v_o} = \left[\frac{\gamma+1}{2+(\gamma-1)M^2}\right]^{1-\frac{1}{\gamma-1}} \left(\frac{P_s}{P_o}\right)_c \left[\frac{(\rho v)_{cr}}{\rho_o v_o}\right]$$

In Moeckel's paper this relationship is written as

$$\frac{A_o}{A_s} = \left(\frac{P_s}{P_o}\right)_c \left[\frac{(\rho v)_{cr}}{\rho_o v_o}\right]$$

or, in other words the quantity

$$\left[\frac{\gamma+1}{2+(\gamma-1)M^2}\right]^{\frac{\gamma}{\gamma-1}}$$

is put equal to 1. This is exact for M = 1.0 but for Mach numbers slightly greater than 1.0 a considerable error is introduced. For example, at M = 1.2 the error is approximately 20%.

From Fig. 14 it can easily be seen that

$$A_s = \frac{y_s - y_{sB}}{\cos \eta}$$

and therefore

$$\frac{y_s - y_{sB}}{\cos \eta} = \left(\frac{P_o}{P_s}\right)_c \left[\frac{\rho_o v_o}{(\rho v)_{cr}}\right] \left[\frac{2 + (\gamma-1)M^2}{\gamma+1}\right]^{\frac{\gamma}{\gamma-1}} y_s = B y_s$$

(In Moeckel's paper the factor $\frac{2 + (\gamma-1)M^2}{\gamma+1}$ is put equal to 1.0 in this equation also.)

Combining terms and simplifying the above equation gives

$$\frac{y_s}{y_{sB}} = \frac{1}{1 - B\cos\eta} \qquad \text{where} \qquad B = \left(\frac{P_o}{P_s}\right)_c \left[\frac{\rho_o v_o}{(\rho v)_{cr}}\right]$$

Now since the sonic line is assumed normal to the average flow direction in its vicinity the inclination of the sonic line is given approximately by the average of its inclination at the shock and at the body $\eta = \frac{1}{2}(\lambda_D + \lambda_s)$.

Knowing y_s / y_{sB}, the value of x_o can be determined, thus fixing the shock wave. From geometrical considerations the quantity L/y_{sB} can also be calculated, where L is the horizontal distance between the sonic point on the body and the shock nose (Fig. 15). The details of this calculation will not be discussed here since they do not involve any further approximations of interest in this discussion.

It is interesting to note, however, that as shown on Fig. 16 Moeckel's method apparently agrees with experimental data. It should be remembered, however, that the location of the sonic point was not given experimentally but was assumed to be located at a point on the body determined by the method suggested by Moeckel and described above.

According to this method the sonic point is located at 78° from the cylinder nose for M = 1.546, and using the data of Fig. 8 ($\frac{L}{d} = 1.36$) the quantity L/y_{sB} can be calculated as follows

$$L = 1.36\, d + r\,(1 - \cos\gamma)$$

$$\eta_{SB} = r \sin \gamma$$

$$\frac{L}{\eta_{SB}} = \frac{2\,(1.36) + (1 - \cos \gamma)}{\sin \gamma}$$

where γ is the angle between the flow direction at ∞ and the radius through the sonic point. If $\gamma = 78^{\circ}$ is used this method gives

$$\frac{L}{\eta_{SB}} = 3.59$$

Moeckel's method of calculation using the continuity equation gives a value of

$$\frac{L}{\eta_{SB}} = 3.60$$

If the measured value of γ is used ($\gamma = 57^{\circ}$) the value of $\frac{L}{\eta_{SB}} = 3.807$ is obtained. This also agrees very closely with Moeckel's predicted values as shown on Fig. 16. For this range of angles (γ), the distance (L) does not change rapidly with γ .

Moeckel also calculated the drag coefficient of two-dimensional bodies with detached shock waves. The drag coefficient calculated by Moeckel included only the drag of the subsonic surfaces and the reference length was again η_{SB}.

If the sonic point is assumed to be at 78° from the stagnation point (Moeckel's theoretical value) the integration of Fig. 11 gives

$$(C_D)_{78^{\circ}} = 1.120$$

If, however, the actual sonic point is used the integration gives

$$(C_D)_{57^{\circ}} = 1.252$$

Both of these values are appreciably different from Moeckel's value

$$(C_D)_M = 0.85$$

for two-dimensional bodies.

This simply means that the method of averaging used by Moeckel does not produce the correct average pressure in the subsonic region.

IV. A THEORETICAL ANALYSIS OF THE FLOW BEHIND A DETACHED SHOCK WAVE

The flow behind a detached shock wave in two dimensions has been discussed by several authors (References 3,4,5,6), some of whose work has been reviewed in section III of this report. Recently, during discussions with Th. von Kármán, he suggested to the author a solution of the problem in the hodograph plane which has so far been carried out only in a simplified form, but which is essentially different in concept from those methods of approach already known. The method suggested by von Kármán will be presented in general and then the approximate treatment will be used to carry out the case of a circular cylinder in a uniform supersonic flow.

1. Fundamental Equations

The basic assumption made in this treatment is the fact that the flow behind such a wave can be considered to be irrotational, thereby making available the mathematical simplicity of linearized equations in the hodograph plane for the two-dimensional case.

With this assumption the equations governing the flow field are (Ref. 11, p. 251)

$$\frac{\partial \phi}{\partial w} = -\frac{1-M^2}{w}\frac{\rho_o}{\rho}\frac{\partial \psi}{\partial \theta}$$

$$\frac{\partial \phi}{\partial \theta} = \frac{\rho_o}{\rho} w \frac{\partial \psi}{\partial w} \qquad (1)$$

where w ~ velocity magnitude, θ ~ velocity direction with respect to undisturbed flow.

Differentiating the first with respect to θ and the second with respect to w gives

$$\phi_{w\theta} = -\frac{1-M^2}{w}\frac{\rho_o}{\rho}\psi_{\theta\theta}$$

$$\phi_{\theta w} = \frac{\rho_o}{\rho} w \psi_{ww} + \frac{\rho_o}{\rho}(1+M^2)\psi_w$$

Now, since $\phi_{w\theta} = \phi_{\theta w}$ where ϕ is a differentiable function of both variables, by subtraction

$$w^2 \psi_{ww} + w(1+M^2)\psi_w + (1-M^2)\psi_{\theta\theta} = 0 \tag{2}$$

or since $M^2 = \dfrac{w^2}{a_o^2 - \frac{\gamma-1}{2} w^2}$ this equation becomes

$$w^2\left(1 - \frac{\gamma-1}{2a_o^2} w^2\right)\psi_{ww} + w\left(1 - \frac{\gamma-3}{2a_o^2} w^2\right)\psi_w + \left(1 - \frac{\gamma+1}{2a_o^2} w^2\right)\psi_{\theta\theta} = 0 \tag{3}$$

It has been shown by Tschapligin that if a solution of this equation is assumed to be of the form

$$\psi = \sum_{\nu=p}^{\infty} F_\nu(w^2)\, w^\nu \left[a_\nu \cos \nu\theta + b_\nu \sin \nu\theta\right] \tag{4}$$

the quantity $F_\nu(w^2)$ is a hypergeometric function satisfying the equation

$$w^2(1-Aw^2)F''(w^2) + \left[\beta - (2A+B)w^2\right]F'(w^2) + \left[\nu^2 C - \nu B - \nu(\nu-1)A\right]F = 0 \tag{5}$$

where A, B, and C are constants.

Thus as long as the series in Eq. (4) is uniformly convergent and the functions F satisfy Eq. (5), then ψ represents the stream function of a plane compressible flow, in a region where the assumptions of irrotational, isentropic flow exist everywhere.

The problem is then reduced to that of evaluating the constants a_ν and b_ν to satisfy a particular set of boundary conditions. It must be remembered that if the assumption of isentropic flow breaks down along a surface within the fluid, the solution cannot be continued across this surface, but the problem must be solved separately for each region in which the assumptions are valid. This is actually the case in the

detached shock wave problem. In this report the flow ahead of the shock wave is assumed to be a uniform two-dimensional flow of known velocity and stagnation conditions. The problem then reduces to a determination of a flow behind the shock wave which can be matched to this uniform flow with a physically possible shock wave.

2. Boundary Conditions at the Body

The boundary conditions for the problems considered by Tschapligin, and those of the present problem, take the same form on the body surface. They consist of a knowledge of the body shape which can be written in intrinsic form as $\theta = \theta(S)$ and

$$\frac{1}{R} = -\frac{\partial \theta}{\partial S} \qquad \text{for } \psi = 0. \tag{6}$$

where R is the local radius of curvature of the body at a point where the body inclination with respect to the direction of undisturbed flow is θ, and S is a coordinate along the surface.

Under the assumption of isentropic irrotational flow this can be expressed in a more useful form by the use of the potential ϕ

$$\frac{1}{R} = -\frac{\partial \phi}{\partial S}\frac{\partial \theta}{\partial \phi} = -w\frac{\partial \theta}{\partial \phi} \tag{7}$$

where ϕ is defined by the relations

$$\frac{\partial \phi}{\partial x} = u \qquad \frac{\partial \phi}{\partial y} = v \qquad \text{and} \qquad u^2 + v^2 = w^2 \tag{8}$$

The quantity $\frac{\partial \theta}{\partial \phi}$ can now be expressed in terms of the stream function ψ by use of Eq.'s (1)

$$d\phi = \frac{\partial \phi}{\partial \theta}d\theta + \frac{\partial \phi}{\partial w}dw = \frac{\rho_o}{\rho} w \frac{\partial \psi}{\partial w} d\theta - \frac{1-M^2}{w}\frac{\rho_o}{\rho}\frac{\partial \psi}{\partial \theta} dw$$

$$d\psi = \frac{\partial \psi}{\partial \theta} d\theta + \frac{\partial \psi}{\partial w} dw$$

solving these equations for $d\theta$ gives

$$d\theta = \frac{\frac{\partial \psi}{\partial w} d\phi + \frac{1-M^2}{w} \frac{\rho_0}{\rho} \frac{\partial \psi}{\partial \theta} d\psi}{\left(\frac{\rho_0}{\rho} w \frac{\partial \psi}{\partial w}^2\right) + \frac{1-M^2}{w} \frac{\rho_0}{\rho} \left(\frac{\partial \psi}{\partial \theta}\right)^2}$$

or

$$\frac{\partial \theta}{\partial \phi} = \frac{\frac{\rho}{\rho_0} \frac{\partial \psi}{\partial w}}{w \left(\frac{\partial \psi}{\partial w}\right)^2 + \frac{1-M^2}{w} \left(\frac{\partial \psi}{\partial \theta}\right)^2} \tag{9}$$

Combining Eq.'s (7) and (9)

$$w \left(\frac{\partial \psi}{\partial w}\right)^2 + \frac{1-M^2}{w} \left(\frac{\partial \psi}{\partial \theta}\right)^2 = -R w \frac{\rho}{\rho_0} \frac{\partial \psi}{\partial w} \qquad \text{on} \qquad \psi = 0 \tag{10}$$

Equations (10) provide a means of determining relationships among the a_ν's and b_ν's, which, for Tschapligin's problem, together with the boundary conditions at infinity should determine all the arbitrary constants in the solution. The difficulty in using this procedure lies in the fact that it is necessary to know the relationship between w and θ on the body, i.e. the curve in the hodograph representing the body surface, and in general this cannot be determined until the solution to the problem is known. The use of this boundary condition will be discussed in more detail in section V.

3. Boundary Conditions at the Shock Wave

Since there is a discontinuity at the shock wave, the flow behind the wave must be determined by boundary conditions at the shock wave rather than at infinity. In the present report, since we are assuming irrotational flow in this region, this boundary condition can be greatly simplified.

In order to match the flow behind the shock to the uniform two-dimensional flow in front, it must be prescribed that the mass flow across any element of the wave shall be preserved. Thus ahead of the wave we have by definition

$$d\eta = \frac{\rho_o}{\rho_\infty U_\infty} d\psi$$

and behind the wave

$$d\eta = \frac{\partial \eta}{\partial \phi} d\phi + \frac{\partial \eta}{\partial \psi} d\psi$$

but since the shock wave can be considered to be a curve in the ϕ, ψ coordinate system

$$d\eta = \left[\frac{\partial \eta}{\partial \phi}\left(\frac{d\phi}{d\psi}\right)_s + \frac{\partial \eta}{\partial \psi}\right] d\psi$$

and the continuity condition can now be prescribed by equating the change in ψ ahead of the wave to that behind the wave. Thus

$$\frac{\rho_o}{\rho_\infty U_\infty} = \frac{\partial \eta}{\partial \phi}\left(\frac{d\phi}{d\psi}\right)_s + \frac{\partial \eta}{\partial \psi}$$

where subscript s refers to conditions immediately behind the shock wave. From the definition of ϕ and ψ this can be written as

$$\frac{\rho_o}{\rho_\infty U_\infty} = \frac{\sin \theta_s}{w_s}\left(\frac{d\phi}{d\psi}\right)_s + \frac{\rho_o}{\rho_s}\frac{\cos \theta_s}{w_s} \qquad (11)$$

Eq. (11) must be satisfied at all points of the shock wave and, since w_s is a known function of θ_s for any given free stream Mach number, this equation provides additional relationships among the arbitrary constants of the general solution (Eq. 4).

4. Approximations

Although these boundary conditions are not complete, they can be

used to arrive at approximate particular solutions which represent the flow near the nose of a body under the detached shock wave flow regime. There are several special body shapes such as the wedge or circular cylinder to which the above method could be applied. In the present paper, however, the method will be somewhat modified before attempting to arrive at a particular solution.

The modification consists of the Tschapligin approximation to the exact hodograph equations (1). By introducing a new variable τ such that

$$d\tau = \sqrt{1-M^2}\,\frac{dw}{w} \tag{12}$$

equations (1) are transformed to

$$\begin{aligned} \phi_\tau &= -\sqrt{1-M^2}\,\frac{\rho_0}{\rho}\,\psi_\theta \\ \phi_\theta &= \sqrt{1-M^2}\,\frac{\rho_0}{\rho}\,\psi_\tau \end{aligned} \tag{13}$$

and by putting $\frac{\rho_0}{\rho}\sqrt{1-M^2}=1$ equations (13) become

$$\begin{aligned} \phi_\tau &= -\psi_\theta \\ \phi_\theta &= \psi_\tau \end{aligned} \tag{14}$$

These are the Cauchy Riemann equations for the function $F = \phi + i\psi$ and the independent variable $\tau - i\theta$.

For convenience of calculation the variable $\tau - i\theta$ is transformed to $\bar{q}$ where $\bar{q} = e^{\tau - i\theta} = q\,e^{-i\theta}$. Thus the Cauchy Riemann equations still hold in terms of q and θ as polar coordinates.

The method by which this Tschapligin transformation simplifies the solution of a given problem is twofold. In the first place the field equation instead of being of the form of Eq. (3) is reduced to

$$\frac{\partial^2\psi}{\partial\tau^2} + \frac{\partial^2\psi}{\partial\theta^2} = 0 \tag{15}$$

Laplace's equation.

The solution of this equation is known to be any analytic function of the complex variable $\tau - i\theta$ or $q e^{-i\theta}$.

Further simplification in the solution of a problem is also afforded by the well-known analogy to the theory of incompressible fluids, since solutions of incompressible fluid flow problems also satisfy Laplace's equation in terms of τ_i and θ where

$$d\tau_i = \frac{dq}{q} \tag{16}$$

where q is the velocity of an incompressible fluid in a flow field which is irrotational and isentropic.

By comparing equations (12) and (16) it can easily be seen that the velocity of a compressible fluid (w) can be written in terms of the velocity of an incompressible fluid by the relationship

$$\frac{dq}{q} = \sqrt{1-M^2}\,\frac{dw}{w} \tag{17}$$

This method was first used by Tschapligin and later improved by von Kármán and Tsien (Ref. 11). The details are well known and will not be discussed here except to show their application to the special problem of flow about a circular cylinder (section V).

Integration of Eq. (17) under the Tschapligin assumption yields

$$\frac{q}{a_o} = \frac{2\,\frac{w}{a_o}}{1+\sqrt{1+\left(\frac{w}{a_o}\right)^2}} \tag{18}$$

where a_o is the velocity of sound at the stagnation point. Fig. 17 is a plot of $\frac{q}{a_o}$ vs $\frac{w}{a_o}$.

If this equation is solved for $\frac{w}{a_o}$ it gives

$$\frac{w}{a_o} = \frac{4\,q/a_o}{4-(q/a_o)^2}$$

The method of solution of a compressible flow problem then consists of taking the known incompressible fluid solution and determining the velocities of the compressible fluid from these formulas. This procedure is somewhat more involved in the present case since the conditions at infinity for the incompressible problem have no exact analogy in the detached shock problem. However it will be shown that by leaving the incompressible solution undetermined at infinity, a fictitious condition is supplied by the shock wave boundary condition. This fixes the incompressible problem at infinity in a manner which produces a good approximation to the actual flow in the region between the shock wave and the body, at least in the neighborhood of the stagnation streamline.

The method will be carried out in detail for the case of a blunt body in section V. Before this is done, however, formulas for the detachment distance and shock wave nose curvature will be derived in terms of a solution assumed to be known as a function of q and θ. These quantities are most useful for comparison with experimental data in the form of schlieren pictures, although, from the solution obtained, any other quantity such as velocity or pressure on the body can also be determined.

5. Derivation of Formula for Shock Wave Detachment Distance

Assuming ψ has been determined as a function of w and θ, it is interesting to calculate the shock wave detachment distance (L) as well as the shock wave radius of curvature (R_s) to provide a simple means of comparison of the calculated flow with experiment. The quantity L can be expressed as

$$L = \int_0^L d\chi = \int_{\phi_1}^{\phi_2} \frac{d\phi}{w} = \int_{w_2}^{0} \frac{\partial \phi}{\partial w} \frac{dw}{w} \qquad (19)$$

where the path of integration is along the so-called stagnation streamline from the body stagnation point to the downstream face of the shock nose. Since the flow along this streamline is undeflected, $d\theta = 0$ and therefore the last step in Eq. (19) is valid.

Using the relations of Eq. (1), Eq. (19) can be written as

$$L = \int_0^{w_2} \frac{1-M^2}{w^2} \frac{\rho_0}{\rho} \frac{\partial \psi}{\partial \theta} \, dw$$

or using Eq. (17) and the fact that $\frac{\rho_0}{\rho}\sqrt{1-M^2} = 1$ this equation becomes

$$L = \int_0^{q_2} \frac{1}{w} \frac{\partial \psi}{\partial \theta} \frac{dq}{q} = \int_0^{\frac{q_2}{a_0}} \frac{4-\left(\frac{q}{a_0}\right)^2}{4a_0 \frac{q}{a_0}} \frac{\partial \psi}{\partial \theta} \frac{d\left(\frac{q}{a_0}\right)}{\frac{q}{a_0}} \tag{20}$$

This equation will be used to calculate L for a circular cylinder once ψ is determined as a function of θ and q.

6. Derivation of Formula for Radius of Curvature of Shock Nose

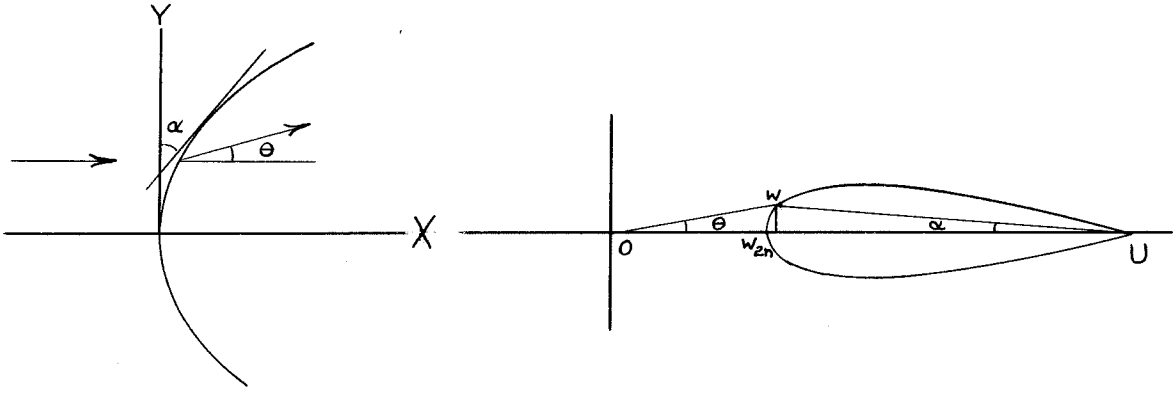

Physical Plane Hodograph Plane

In order to express the shock wave nose curvature in terms of the stream function and its derivatives it is only necessary to use the following relationships which are valid in the region close to the shock nose.

$$\alpha(u - w_{2n}) = \theta w_2 \tag{21}$$

$$\frac{d^2x}{dy^2} = \frac{1}{R_s} \tag{22}$$

$$\frac{dx}{d\eta} = \frac{\eta}{R_s} = \alpha \qquad \text{from symmetry} \qquad (23)$$

$$\theta = \frac{v_2}{u_2} = \frac{1}{u_2}\left[\frac{\partial v}{\partial \eta} d\eta + \frac{\partial v}{\partial x} dx\right] = \frac{1}{u_2} \frac{\partial v}{\partial \eta} \eta \qquad (24)$$

where

R_s - radius of curvature of shock nose

u - free stream velocity

subscript 2 refers to conditions behind shock at an arbitrary point

subscript 2n refers to conditions behind shock at the nose

Combining Eq.'s (21), (23) and (24)

$$\frac{\eta}{R_s}(u - w_{2n}) = \frac{w_2}{u_2} \frac{\partial v}{\partial \eta} \eta$$

or

$$R_s = \frac{(u - w_{2n})}{\frac{\partial v}{\partial \eta}} \qquad \text{since} \quad u_2 \cong w_2 \qquad (25)$$

The quantity ($u - w_{2n}$) can be evaluated in terms of the free stream Mach number from normal shock wave theory since

$$u - w_{2n} = u\left(1 - \frac{w_{2n}}{u}\right) = u\left(1 - \left(\frac{a^*}{u}\right)^2\right) = u\left[1 - \frac{\gamma-1}{\gamma+1}\left(1 + \frac{2}{(\gamma-1)M^2}\right)\right]$$

$$u - w_{2n} = U \frac{2}{\gamma+1}\left(\frac{M^2-1}{M^2}\right) \qquad (26)$$

The quantity $\frac{\partial v}{\partial \eta}$ can be expressed in terms of ψ and its derivatives by considering v as a function of ϕ and ψ . Since

$$\frac{\partial v}{\partial \eta} = \frac{\partial v}{\partial \phi} \frac{\partial \phi}{\partial \eta} + \frac{\partial v}{\partial \psi} \frac{\partial \psi}{\partial \eta} \qquad (27)$$

and

$$d\phi = \frac{\partial \phi}{\partial u} du + \frac{\partial \phi}{\partial v} dv$$

$$d\psi = \frac{\partial \psi}{\partial u} du + \frac{\partial \psi}{\partial v} dv$$

Then solving for dv gives

$$dv = \frac{\frac{\partial \psi}{\partial u} d\phi - \frac{\partial \phi}{\partial u} d\psi}{\frac{\partial \phi}{\partial u}\frac{\partial \psi}{\partial v} - \frac{\partial \phi}{\partial v}\frac{\partial \psi}{\partial u}}$$

or

$$\frac{\partial v}{\partial \phi} = \frac{\frac{\partial \psi}{\partial u}}{\frac{\partial \phi}{\partial u}\frac{\partial \psi}{\partial v} - \frac{\partial \phi}{\partial v}\frac{\partial \psi}{\partial u}}$$

and (28)

$$\frac{\partial v}{\partial \psi} = - \frac{\frac{\partial \phi}{\partial u}}{\frac{\partial \phi}{\partial u}\frac{\partial \psi}{\partial v} - \frac{\partial \phi}{\partial v}\frac{\partial \psi}{\partial u}}$$

Inserting (28) into (27)

$$\frac{\partial v}{\partial y} = \frac{\frac{\partial \psi}{\partial u}\frac{\partial \phi}{\partial y} - \frac{\partial \phi}{\partial u}\frac{\partial \psi}{\partial y}}{\frac{\partial \phi}{\partial u}\frac{\partial \psi}{\partial v} - \frac{\partial \phi}{\partial v}\frac{\partial \psi}{\partial u}} = \frac{v\frac{\partial \psi}{\partial u} - \frac{\rho}{\rho_o} u \frac{\partial \phi}{\partial u}}{\frac{\partial \phi}{\partial u}\frac{\partial \psi}{\partial v} - \frac{\partial \phi}{\partial v}\frac{\partial \psi}{\partial u}} \qquad (29)$$

The derivatives with respect to u and v in this expression can now be written in terms of w by the relationship

$$u^2 + v^2 = w^2$$

$$\frac{u}{v} = \tan \theta$$

After this change of variable Eq. (29) becomes

$$\frac{\partial v}{\partial y} = \frac{w^2\left(\frac{\rho_2}{\rho_o}\right)}{\left(\frac{\partial \psi}{\partial \theta}\right)_2} \qquad \text{for} \quad \theta = 0$$

and therefore from Eq. (25)

$$R_s = \frac{2}{\gamma+1}\,\frac{U}{w_2^2}\,\frac{M^2-1}{M^2}\left(\frac{\partial\psi}{\partial\theta}\right)_2\left(\frac{\rho_o}{\rho}\right)_2 \qquad (30)$$

V. SOLUTION FOR CIRCULAR CYLINDER

Since experimental data on circular cylinders was available for comparison with the theory, the method described was applied to a body with a radius of curvature R, where R is a constant independent of θ.

It is well known that for an incompressible fluid the complex potential $F = \phi + i\psi$ for a circular cylinder can be written as

$$F = ab\left\{\frac{2 - \frac{\bar{q}}{a}}{\sqrt{1 - \frac{\bar{q}}{a}}}\right\} \tag{31}$$

where a and b are arbitrary constants to be determined by the boundary conditions.

1. Boundary Condition at Stagnation Point

In order to satisfy the boundary condition R = constant on the body it is necessary to insert (31) into (10). This means the quantities $\frac{\partial \psi}{\partial w}$ and $\frac{\partial \psi}{\partial \theta}$ must be determined. To do this simply, the function F is put in a more convenient form by expanding it in a series, valid for small values of q or w and θ close to $\pi/2$. Then the boundary condition (10) is satisfied at the stagnation point.

Expanding F in a series in $\bar{q} = q e^{-i\theta}$

$$\frac{F}{ab} = 2 + \frac{1}{4}\left(\frac{q}{a}\right)^2 \cos 2\theta - \frac{1}{16}\left(\frac{q}{a}\right)^3 \cos 3\theta + \ldots + i\left[-\frac{1}{4}\left(\frac{q}{a}\right)^2 \sin 2\theta + \frac{1}{16}\left(\frac{q}{a}\right)^3 \sin 3\theta + \ldots\right]$$

and thus

$$\psi = -\frac{ab}{4}\left(\frac{q}{a}\right)^2 \sin 2\theta - \frac{ab}{4}\left(\frac{q}{a}\right)^3 \sin 3\theta + \ldots$$

To simplify this expression further put $\theta = \frac{\pi}{2} - \theta^*$ and expand in terms of θ^*. This gives

$$\psi = -\frac{ab}{2}\left(\frac{q}{a}\right)^2\theta^* + \frac{ab}{4}\left(\frac{q}{a}\right)^3 + \frac{ab}{3}\left(\frac{q}{a}\right)^2\theta^{*3} - ab\frac{9}{8}\left(\frac{q}{a}\right)^3\theta^{*2} + \ldots \quad (32)$$

Since on the body $\psi = 0$ and it can be shown that q is of the same order as θ^*, if the hodograph representation of the body is considered, then for small values of q and θ^*

$$\theta^* = \frac{1}{2}\frac{q}{a} \qquad \text{as a first approximation.} \quad (33)$$

From Eq. (32) differentiating with respect to θ

$$\frac{\partial\psi}{\partial\theta} = \frac{ab}{2}\left(\frac{q}{a}\right)^2 - ab\left(\frac{q}{a}\right)^2\theta^{*2} - ab\frac{9}{16}\left(\frac{q}{a}\right)^3\theta^* + \ldots$$

and differentiating with respect to q

$$\frac{\partial\psi}{\partial q} = -b\frac{q}{a}\theta^* + b\cdot\frac{3}{4}\left(\frac{q}{a}\right)^2 + b\frac{2}{3}\frac{q}{a}\theta^{*3} + b\frac{27}{32}\left(\frac{q}{a}\right)^2\theta^{*2} + \ldots$$

Now using (33)

$$\frac{\partial\psi}{\partial\theta} = \frac{ab}{2}\left(\frac{q}{a}\right)^2 - \frac{ab}{4}\left(\frac{q}{a}\right)^4 - ab\frac{9}{64}\left(\frac{q}{a}\right)^4 + \ldots \quad (34)$$

$$\frac{\partial\psi}{\partial q} = \frac{b}{4}\left(\frac{q}{a}\right)^2 + \frac{b}{12}\left(\frac{q}{a}\right)^4 + b\frac{27}{128}\left(\frac{q}{a}\right)^4 \quad (35)$$

Now since $\frac{dq}{dw} = 1$ near $w = 0$, $\frac{\partial\psi}{\partial q} = \frac{\partial\psi}{\partial w}$.

From the form of Eq.'s (34) and (35) it can be seen that inserting them into Eq. (10) and equating coefficients of like powers of q will give relationships of the form

$$\frac{1}{w}\left(\frac{ab}{2}\right)^2\frac{q^4}{a^4} = Rw\frac{b}{4}\frac{q^2}{a^2}$$

and, since near $w = 0$ $q = w$, this gives

$$b = R \tag{36}$$

in the limit as $q \to w \to 0$.

Thus one of the two arbitrary constants has been evaluated and it now remains to evaluate "a", the remaining constant in the assumed solution.

2. Boundary Condition at the Shock Wave

In order to assure the continuity of mass flow across the shock wave, Eq. (11) must be satisfied at all points along the wave.

In a manner similar to that used near the body stagnation point, the complex function $F(\bar{q})$ is expanded in a series. This series, however, is convergent in a region near the shock nose where the velocities have the value $\bar{q}_{2n}$ or $\bar{w}_{2n}$. Thus the Taylor series in $(\bar{q} - q_{2n})$ can be separated into its real and imaginary parts and the result is of the form

$$\phi = \frac{2 - \frac{q_{2n}}{a}}{\sqrt{1 - \frac{q_{2n}}{a}}} + \frac{\frac{q_{2n}}{a}\left(\frac{q - q_{2n}}{a}\right)}{2\left(1 - \frac{q_{2n}}{a}\right)^{3/2}} - \frac{\left(\frac{q_{2n}}{a}\right)^2\left(2 + \frac{q_{2n}}{a}\right)}{8\left(1 - \frac{q_{2n}}{a}\right)^{5/2}}\theta^2 + \cdots \tag{37}$$

$$\psi = \frac{-\left(\frac{q_{2n}}{a}\right)^2}{2\left(1 - \frac{q_{2n}}{a}\right)^{3/2}}\theta + \cdots \tag{38}$$

The quantity $(q - q_{2n})$ which occurs in the expression for ϕ must now be expressed in the same approximate form as the rest of the expansion. To do this it is necessary to use the approximation to the oblique shock relations for small flow deflections (θ) and shock inclinations (α).

To arrive at this relationship the following exact equations for oblique shocks are used

$$\tan \alpha = \frac{w_2 \sin \theta}{u - w_2 \cos \theta} \tag{39}$$

$$u_1 w_2 \cos \alpha \cos(\alpha + \theta) = a^{*2} - \frac{\gamma - 1}{\gamma + 1} u_1^2 \sin^2 \alpha \tag{40}$$

where α is defined on the sketch

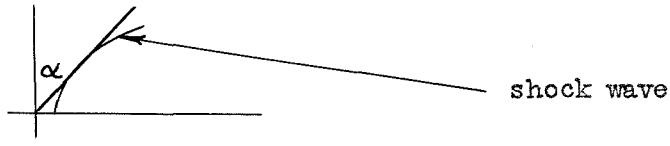

Since $\alpha \to 0$ and $w \to 0$ in the neighborhood of the shock nose these relationships can be expanded in terms of θ giving

$$\frac{w - w_{2n}}{a_o} = \frac{\frac{w_{2n}}{a_o}}{2\left(1 - \frac{w_{2n}}{u}\right)} \left[\left(\frac{w_{2n}}{u}\right)^2 + 1 - 2 \frac{\gamma - 1}{\gamma + 1} \frac{w_{2n}}{u} \right] \theta^2 = K_w \theta^2 \tag{41}$$

Using this and Eq. (17) the quantity $(q - q_{2n})$ can then be found in the form

$$\frac{q - q_{2n}}{a_o} = K_q \theta^2 \tag{42}$$

Then, symbolically, Eq.'s (37) and (38) are of the form

$$\begin{aligned} \phi &= A + B\theta^2 \\ \psi &= C\theta \end{aligned} \tag{43}$$

where A, B, and C are, by Eq.'s (37), (38) and (42), as follows

$$A = \frac{2 - q_{2n}}{\sqrt{1 - \frac{q_{2n}}{a}}} \tag{44}$$

$$B = \frac{\frac{q_{2n}}{a} K_q \frac{a_o}{a}}{2\left(1 - \frac{q_{2n}}{a}\right)^{3/2}} - \frac{\left(\frac{q_{2n}}{a}\right)^2 \left(2 + \frac{q_{2n}}{a}\right)}{8\left(1 - \frac{q_{2n}}{a}\right)^{5/2}}$$

$$C = - \frac{\left(\frac{q_{2n}}{a}\right)^2}{2\left(1 - \frac{q_{2n}}{a}\right)^{3/2}}$$

In terms of these constants

$$\left(\frac{d\phi}{d\psi}\right)_s = \frac{2B}{C} \tag{45}$$

Eq. 11 can now be written in an approximate form for small values of θ and α (i.e. near the shock nose).

$$\frac{\rho_o}{\rho_\infty U_\infty} = \frac{1}{W_2} \frac{\rho_o}{\rho_2} + \frac{1}{W_2} G\theta^2 + \frac{1}{W_2} \frac{2B}{C} \theta^2 + \cdots \tag{46}$$

where $\frac{1}{W_2} \frac{\rho_o}{\rho_2} + \frac{1}{W_2} G\theta^2$ comes from the term $\frac{\rho_o}{\rho_2} \frac{\cos \theta_s}{W_s}$ when expanded in series. In this expression

$$G = \frac{\left(\frac{W_{2n}}{a_o}\right) K_W}{\sqrt{1 + \left(\frac{W_{2n}}{a_o}\right)^2}} - \frac{\rho_o}{\rho_2} \left(\frac{1}{2} + \frac{K_W}{\left(\frac{W_{2n}}{a_o}\right)}\right) \tag{47}$$

Eq. (46) must hold for all values of θ within the domain of convergence and therefore the coefficients of θ^n must be zero for all values of $n > 1$. This gives us the equation which determines the remaining arbitrary constant "a."

$$G + \frac{2B}{C} = 0$$

or

$$G - \frac{2K_q}{\frac{q_{2n}}{a_o}} + \frac{\left(2 + \frac{q_{2n}}{a}\right)}{2\left(1 - \frac{q_{2n}}{a}\right)} = 0$$

or

$$\frac{q_{2n}}{a} = \frac{4Kq - 2G\frac{q_{2n}}{a_o} - 2\frac{q_{2n}}{a_o}}{4Kq - 2G\frac{q_{2n}}{a_o} + \frac{q_{2n}}{a_o}} \tag{48}$$

Fig. 18 is a plot of $\frac{a}{a_o}$ vs M (free stream Mach number).

This is the desired equation for "a". Both arbitrary constants in the assumed general solution have now been evaluated and a possible flow field has been found which satisfies those boundary conditions which have been discussed. It remains to determine how closely this flow resembles the actual flow behind a detached shock wave created by a circular cylinder.

To do this the function F is simply substituted into equations (20) and (30) for the detachment distance and the shock wave radius of curvature.

These quantities were calculated for a range of Mach numbers and compared with the same quantity as given by other theories and with experimental data obtained at the Jet Propulsion Laboratory as discussed previously in this report. The comparison is made on Figs. 13 and 14. From this comparison it appears that the method presented here gives a good approximation to the flow field around a circular cylinder, especially at higher free stream Mach numbers. The discrepancy which exists is attributable to the fact that in the compressible fluid field, the body streamline deviates considerably from the circular cylinder shape. The actual body produced by this stream function is considerably thinner than a circular cylinder of radius "b".

VI. DISCUSSION

1. Experiments

Until recently, experimental data on the detached shock wave phenomenon consisted of a few pictures, showing the wave ahead of spherical shells fired from guns. Very little was known about the flow in the region between the wave and the body or about the pressures on the body. Recently, however, some experiments have been performed by Ladenburg with the use of an interferometer (Ref. 7) and by Liepmann with a schlieren system (Ref. 9). This work was done not as an investigation of the detached shock wave phenomenon itself but, in each instance, the data were produced as a result of the investigation of some allied or related problem. It served, however, to give an impetus to theoretical investigators, and as a result several theories were produced which attempted to predict such quantities as shock wave shape and position.

As is usually the case in a new field of investigation the first investigators attempted to simplify the problem by various assumptions which made the mathematics more tractable. The scarcity of experimental data made it difficult, if not impossible, to determine which of these simplifying assumptions were justified and which caused large errors in the results.

The present report, which is the result of an investigation primarily concerned with the detached shock wave flow regime, has succeeded, by comparison of theory and experiment, in showing the physical importance of various parameters involved in the problem.

2. Nagamatsu Theory

The fact that the flow in the vicinity of the body nose is subsonic has led some investigators to make approximations which under less critical conditions would produce excellent results. For example Naga-

matsu has used the so-called Prandtl-Glauert rule which has been derived from consideration of the linearized subsonic equations. Since the flow in the subsonic field behind a detached wave has velocities varying from sonic to zero and since for blunt bodies the flow actually changes direction by 90°, this assumption does not produce results in agreement with experiment as shown on Fig. 13. The theory was nevertheless useful in that it served to stimulate thought and perhaps was responsible for many of the later ideas on the subject.

3. Moeckel Theory

The theory devised by Moeckel is an attempt to solve the practical problem of determination of the drag of the body without consideration of the detailed flow phenomenon in the subsonic region.

The fact that the relationship between the sonic line and the shock wave is given correctly by this theory and that it does seem to be independent of the body shape ahead of the sonic point is very interesting and serves to show the importance of the body shape throughout the entire subsonic field. In other words two slightly different body shapes could conceivably produce greatly different sonic point locations with respect to their leading edges. Thus the detachment distance would also be very different for each of these bodies although the bodies themselves are almost identical. This explains the lack of correlation of shock detachment for the theory presented in section V with experiment. The shape of the body corresponding to the stream function used in the example worked out in V is not a circular cylinder but departs from this shape, by a factor proportional to $\frac{w}{q}$. This will be discussed in more detail later.

4. Lin, Shen, Rubinov Theory

The method of Lin, Shen and Rubinov is an attempt to find a solu-

tion to the detached shock wave problem for blunt bodies without the simplification of the assumption of irrotationality for the flow behind the wave. The method makes use of power series expansions for the body and shock wave shape, thus restricting it to bodies whose shape can be expressed locally by analytic functions. Since the basic equations are non-linear, the exact solution can be represented only by the entire series, and the use of a finite number of terms gives a good approximation to the exact solution only in a region where the series is absolutely and uniformly convergent, and where this convergence is extremely rapid.

This question of convergence cannot be answered in mathematically precise terms but only by a physical argument based upon the existence of singularities within the body. The body shape cannot be determined at distances very far from the nose and therefore it is not known to what body the resulting flow corresponds. The method is very interesting and will perhaps lead to further work with the exact differential equations, which would be extremely valuable, especially for high Mach numbers, where the vorticity plays an important role.

5. Hodograph Method

The method presented in section V makes use of the simplification afforded by the assumption of irrotationality and is also restricted to two-dimensional flow. Unfortunately time did not permit the carrying out of the necessary experiments to properly compare with the special example worked out under this theory. The comparison of Fig. 13 is based on the radius of curvature of the nose of the body which has been shown to be a poor choice. The flow is more sensitive to the body shape near the sonic point than to the shape near the stagnation point, and therefore the theory should be made to conform to the experimental set-

up in this region, rather than at the stagnation point.

It can easily be shown that the quantity b is equal to R only at the stagnation point and that $R = b\frac{dq}{dw}$ for other points along the body. Thus R is decreasing as the flow accelerates, producing a body shape considerably thinner than a circular cylinder. The theory can be made to give a body more closely resembling a circular cylinder by introducing more arbitrary constants into the function F and evaluating them by fur further expansion of the boundary conditions on the body.

The more exact treatment discussed in section IV involving the use of hypergeometric functions also appears feasible and should give excellent results at Mach numbers where the vorticity can be neglected.

In conclusion it should be pointed out that this method is not restricted to blunt bodies and can be applied to wedge-shaped airfoils.

REFERENCES

1. Foelsch, K. "A New Method of Designing Two-Dimensional Laval Nozzles for a Parallel and Uniform Jet." Report NA-46-235, North American Aviation Company, Inc.

2. Gompf, George. "Supersonic Nozzle Design for Viscous Fluids." Thesis. Pasadena. California Institute of Technology, 1949.

3. Nagamatsu, H.T. "Theoretical Investigation of Detached Shock Waves." Thesis. Pasadena. California Institute of Technology, 1949.

4. Lin, C.C. and Rubinov, S.I. "On the Flow Behind Curved Shocks." Journal of Mathematics and Physics, July 1948.

5. Lin, C.C. and Shen, S.F. "An Analytic Determination of the Flow Behind a Symmetrical Curved Shock in a Uniform Stream." Unpublished report.

6. Dugundji, John. "An Investigation of the Detached Shock in Front of a Body of Revolution." Journal of Aeronautical Sciences, December, 1948.

7. Ladenburg, R.; Van Voorhis, C.C.; and Windkler, J. "Interferometric Study of Supersonic Phenomena." Navord Reports 69-46, Part I, 93-46, Part II, 7-47, Part III.

8. Moeckel, W.E. "Approximate Method of Predicting Form and Location of Detached Shock Waves Ahead of Plane or Axially Symmetric Bodies." NACA Technical Note 1921, July 1949.

9. Liepmann, Hans Wolfgang; Ashkenas, Harry; and Cole, Julian D. "Experiments in Transonic Flow." Tech. Report No. 5667, Air Materiel Command, U.S. Air Forces, February 19, 1948. Prepared by C.I.T., June 1947, under AAF Contract No. W33-038ac-1717 (11592).

10. Courant, Friedrichs. "Supersonic Flow and Shock Waves." Interscience Publishers.

11. Tsien, H.S. "Two-Dimensional Subsonic Flow of Compressible Fluids." Journal of Aeronautical Sciences, 6, 399, 1939.

12. Maccoll, J.W. and Codd, J. "Theoretical Investigations of the Flow Around Various Bodies in the Sonic Region of Velocities." Theor. Res. Report No. 17/45 Armament Research Dept. British M.O.S. September 1945.

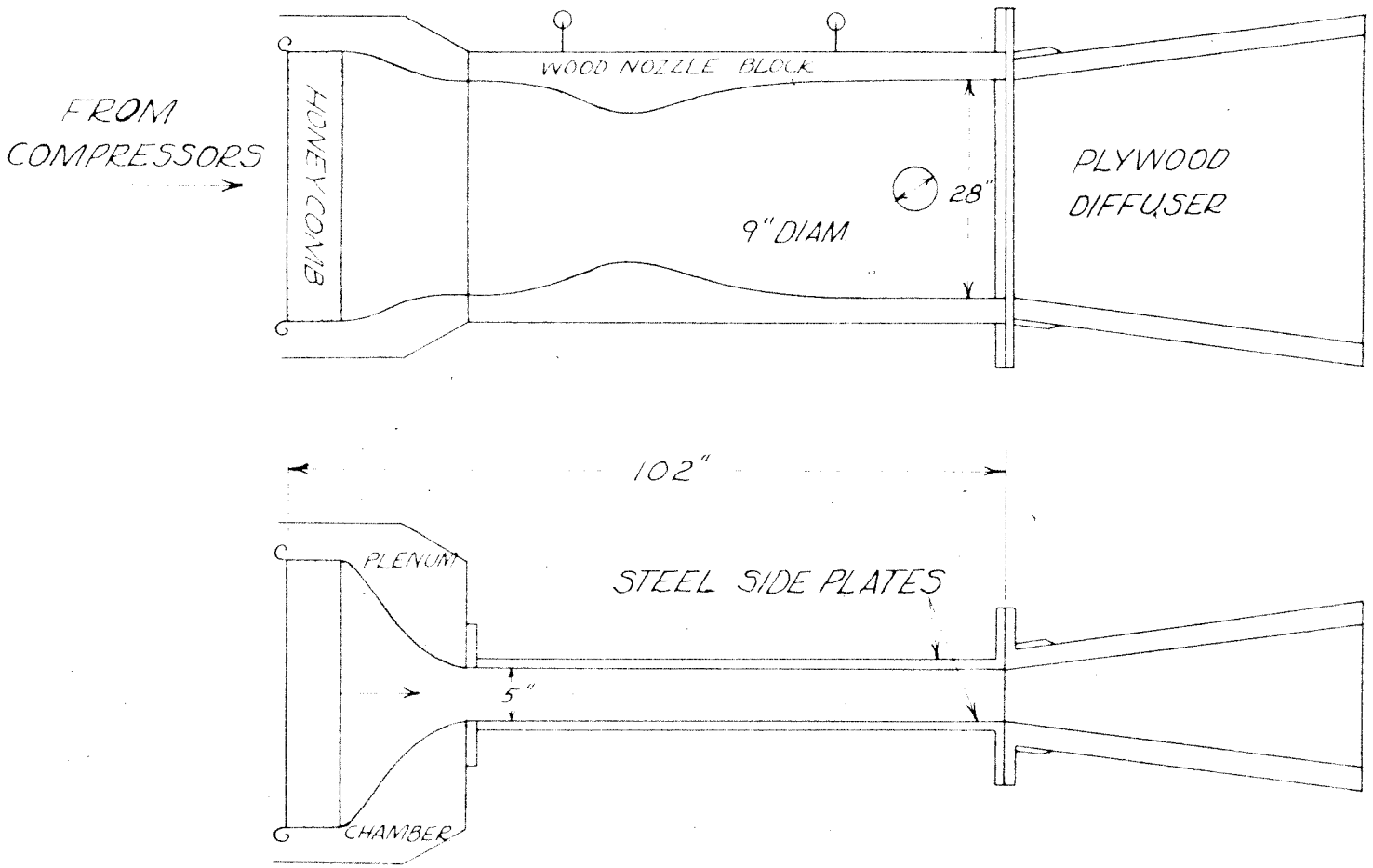

Fig. 1. Schematic Sketch of Two-Dimensional Supersonic Wind Tunnel

Jet Propulsion Laboratory - California Institute of Technology

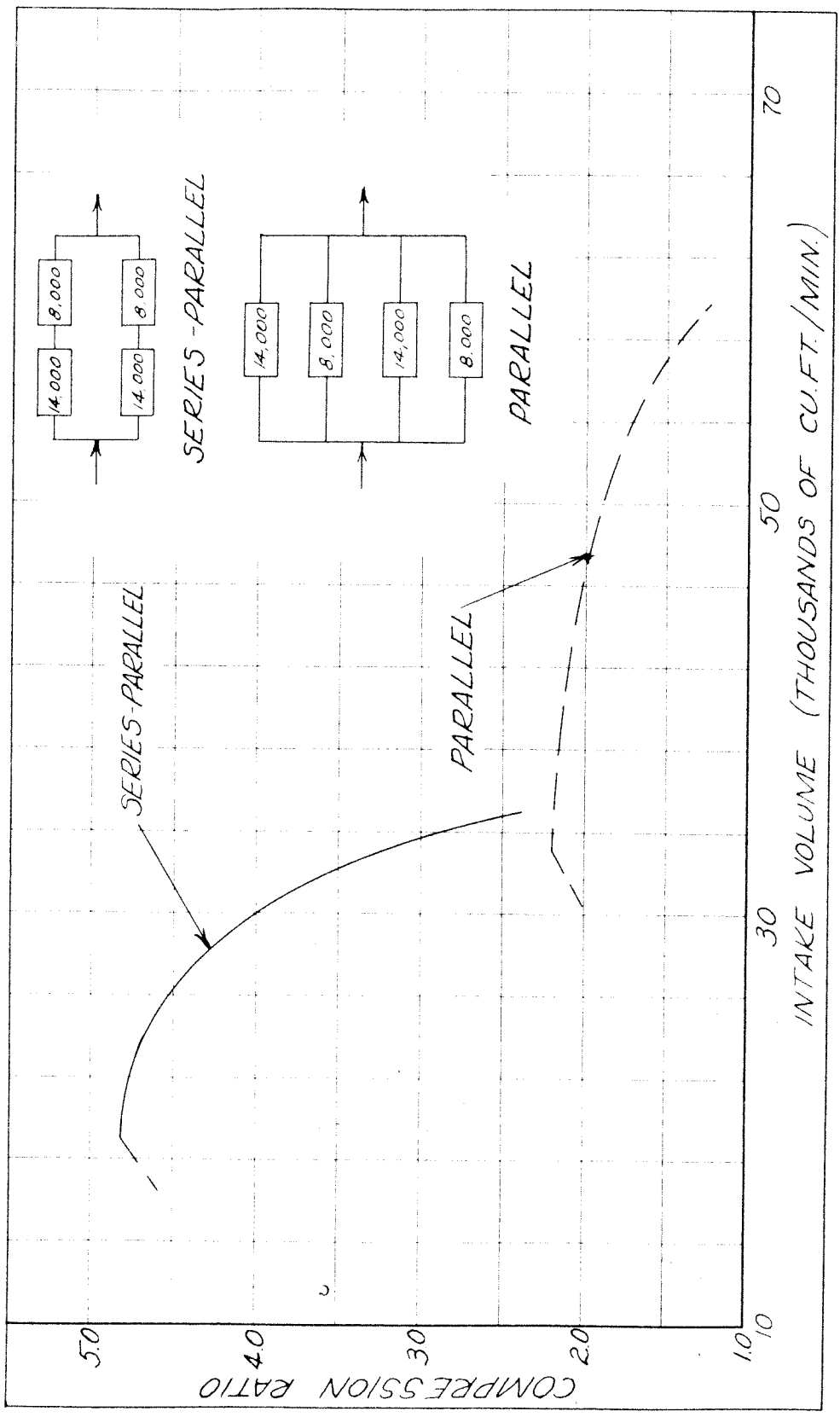

Fig. 2. Compressor Performance

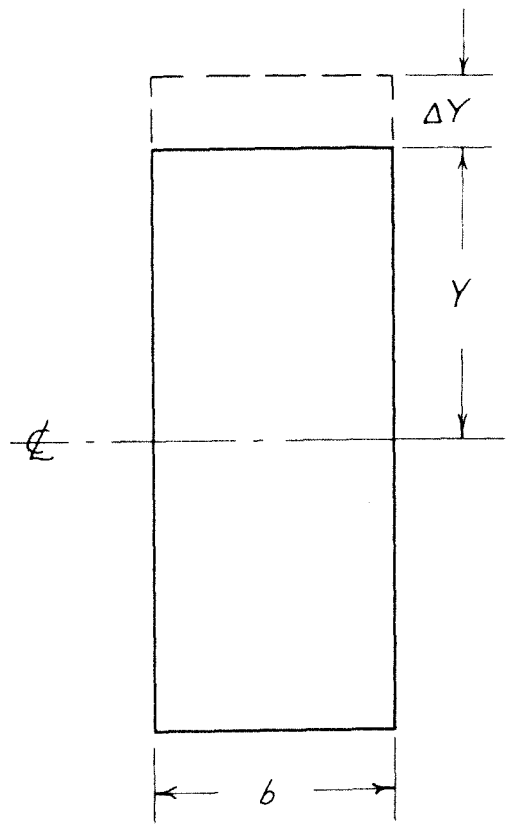

Fig. 5. Notation for Nozzle Design Equations

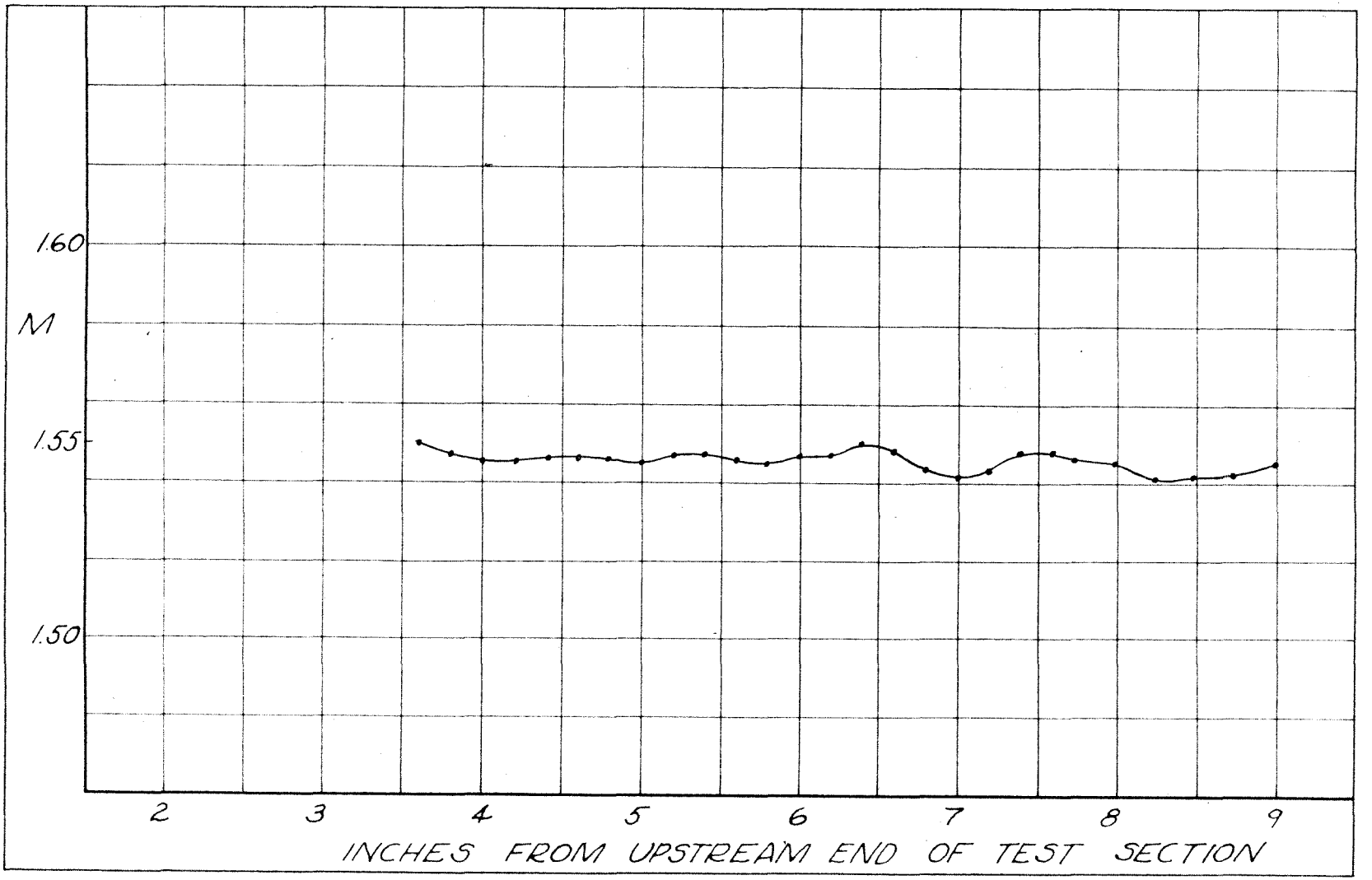

Fig. 4. Mach Number Distribution in Test Section of Two-Dimensional Wind Tunnel

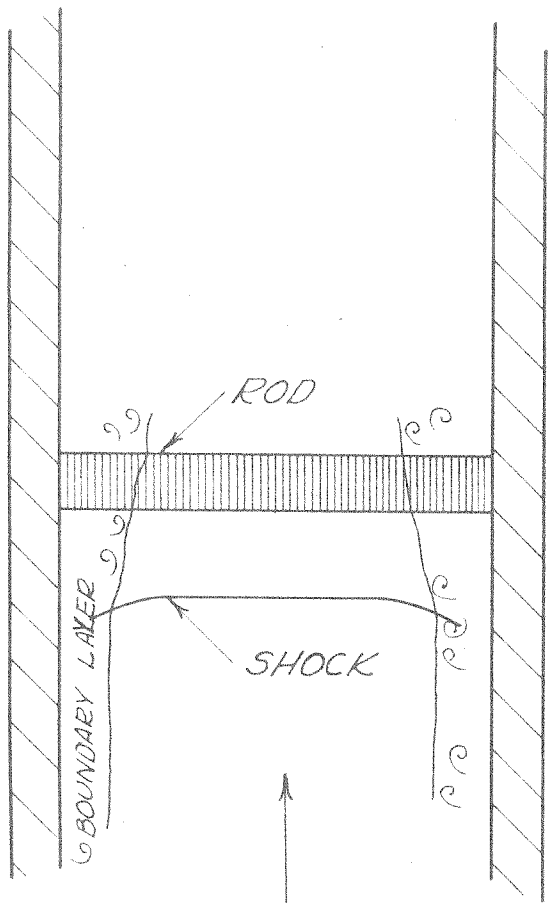

(a)

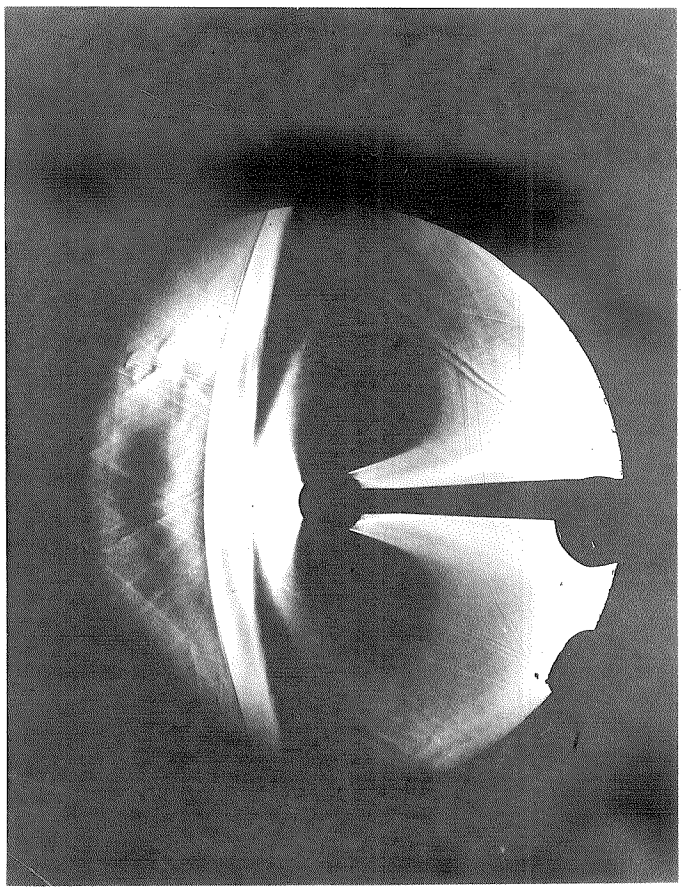

(b)

Fig. 5. 3/4" Diameter Cylinder 5" Span

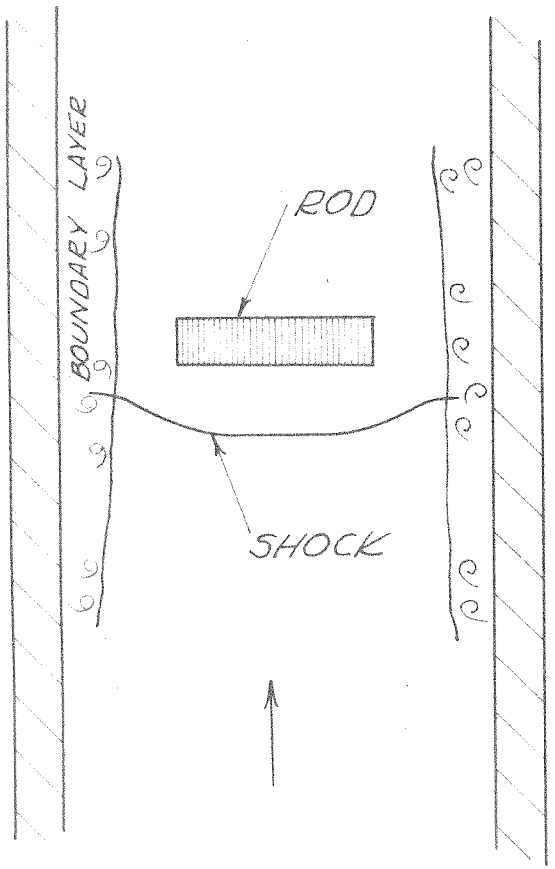

(a)

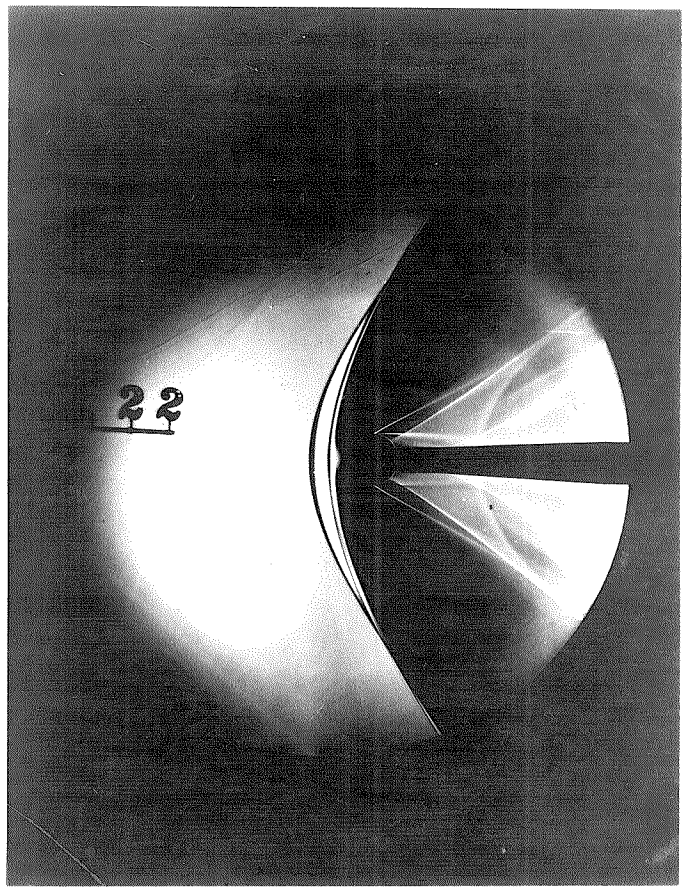

(b)

Fig. 6. 3/4" Diameter Cylinder 2.0" Span

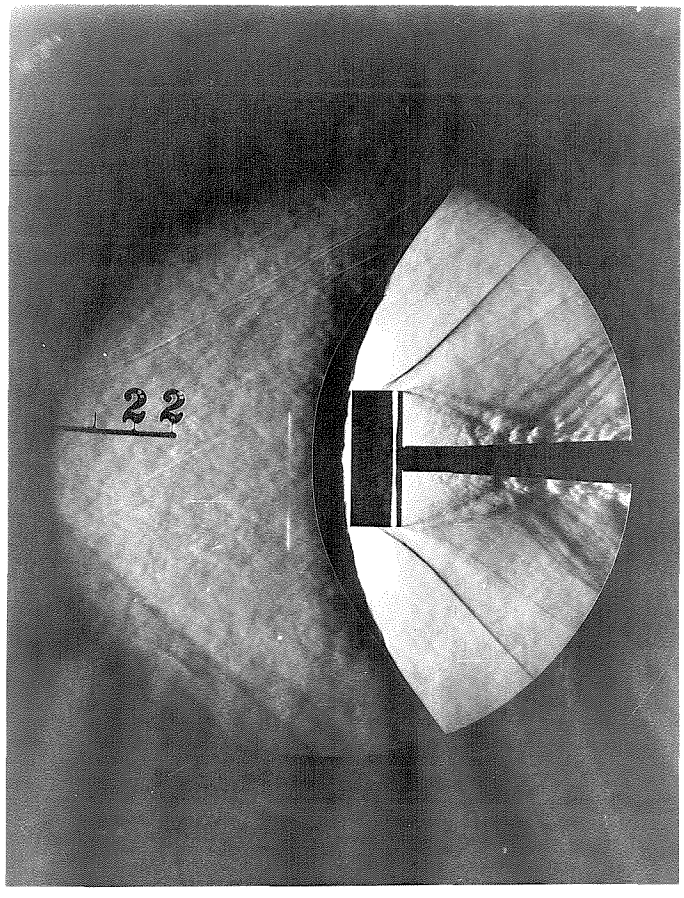

Fig. 7.

Schlieren Picture

Circular Cylinder Mounted Vertically in the

Two-Dimensional Wind Tunnel

M = 1.546

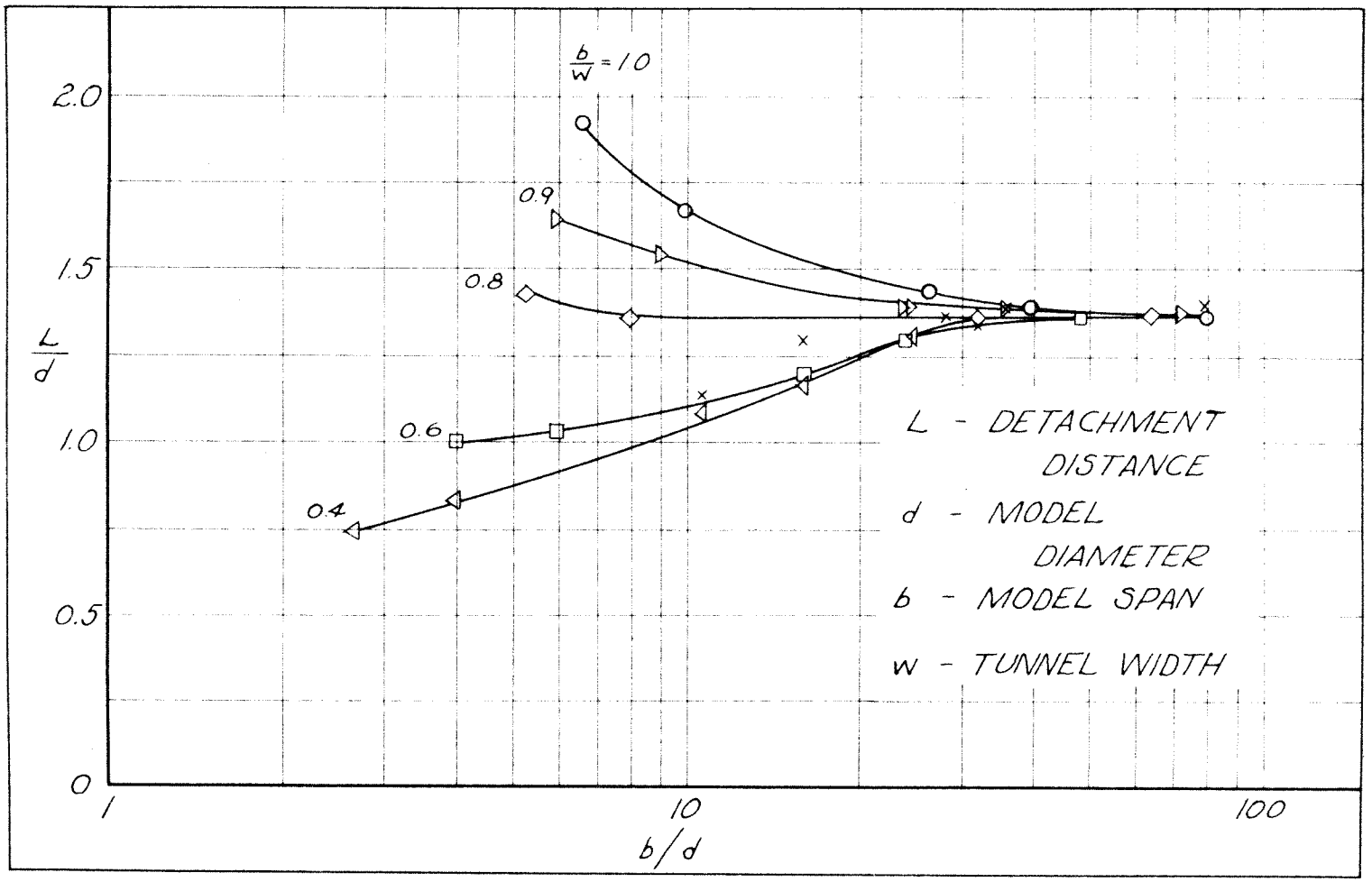

Fig. 8. Shock Wave Detachment Distance vs Model Span for Circular Cylinders at M = 1.846

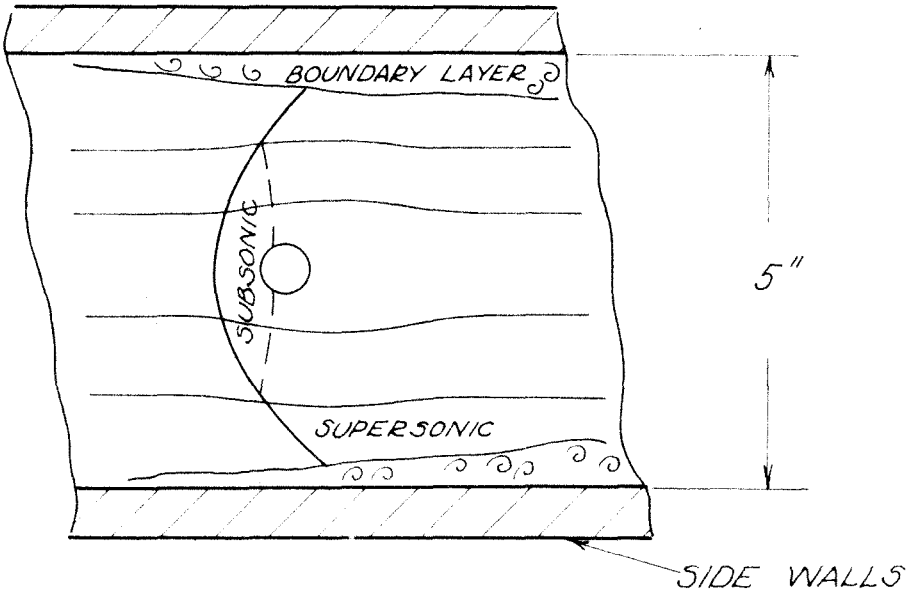

Fig. 9.

Plan View of

Circular Cylinder Mounted Vertically in the

Wind Tunnel

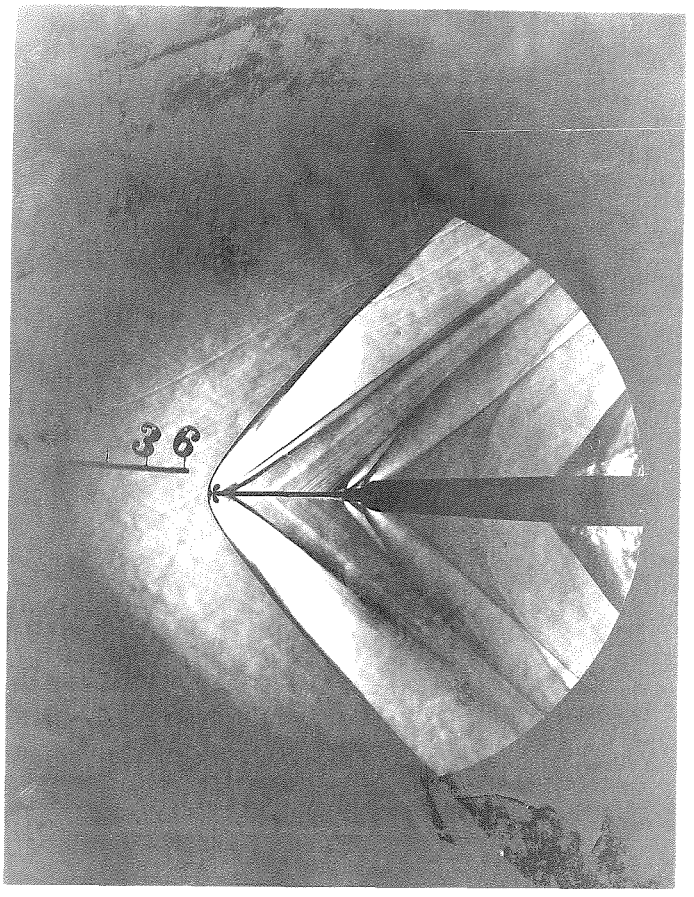

Fig. 10.

Two-Dimensional Shock Wave

for Circular Cylinder

M = 1.546

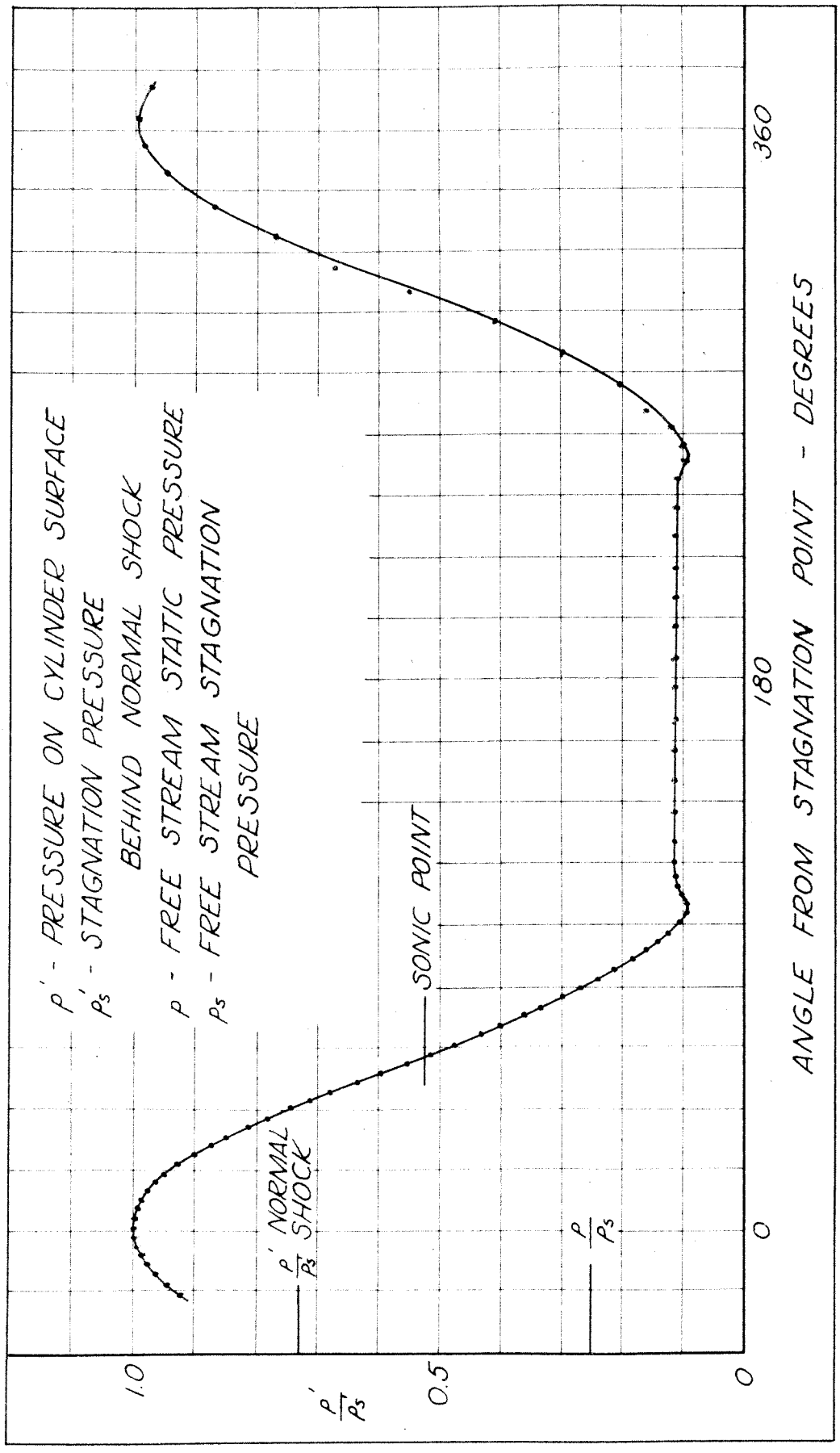

Fig. 11. Pressure Distribution Around a Circular Cylinder

Fig. 12.

Circular Cylinder in Vertical Position

Showing Two-Dimensional Shock

M = 1.546

Dark vertical band - cylindrical model

Light vertical band - shock wave

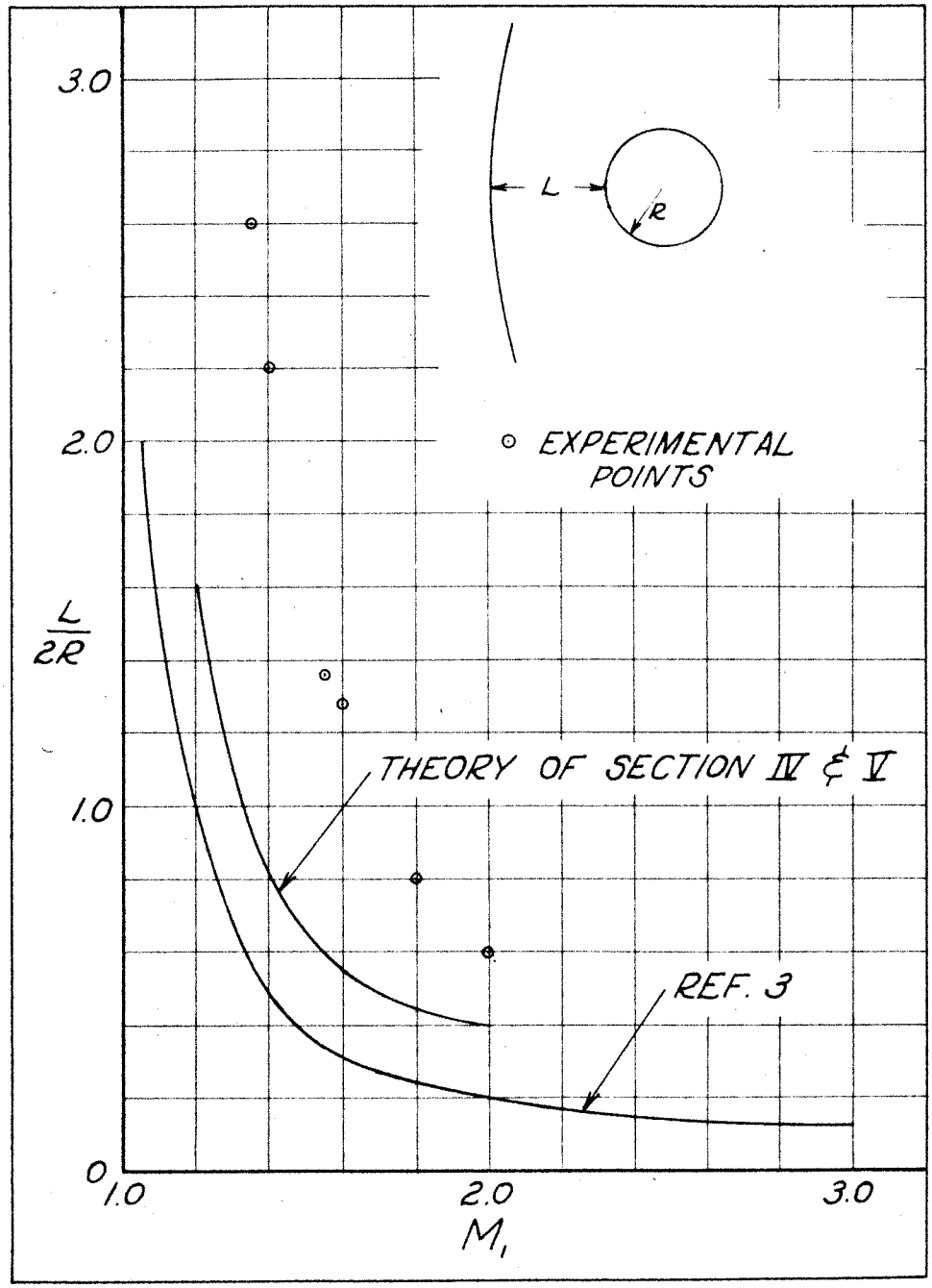

Fig. 13. Comparison of Theory (Ref. 3 and Section IV) with Experimental Data

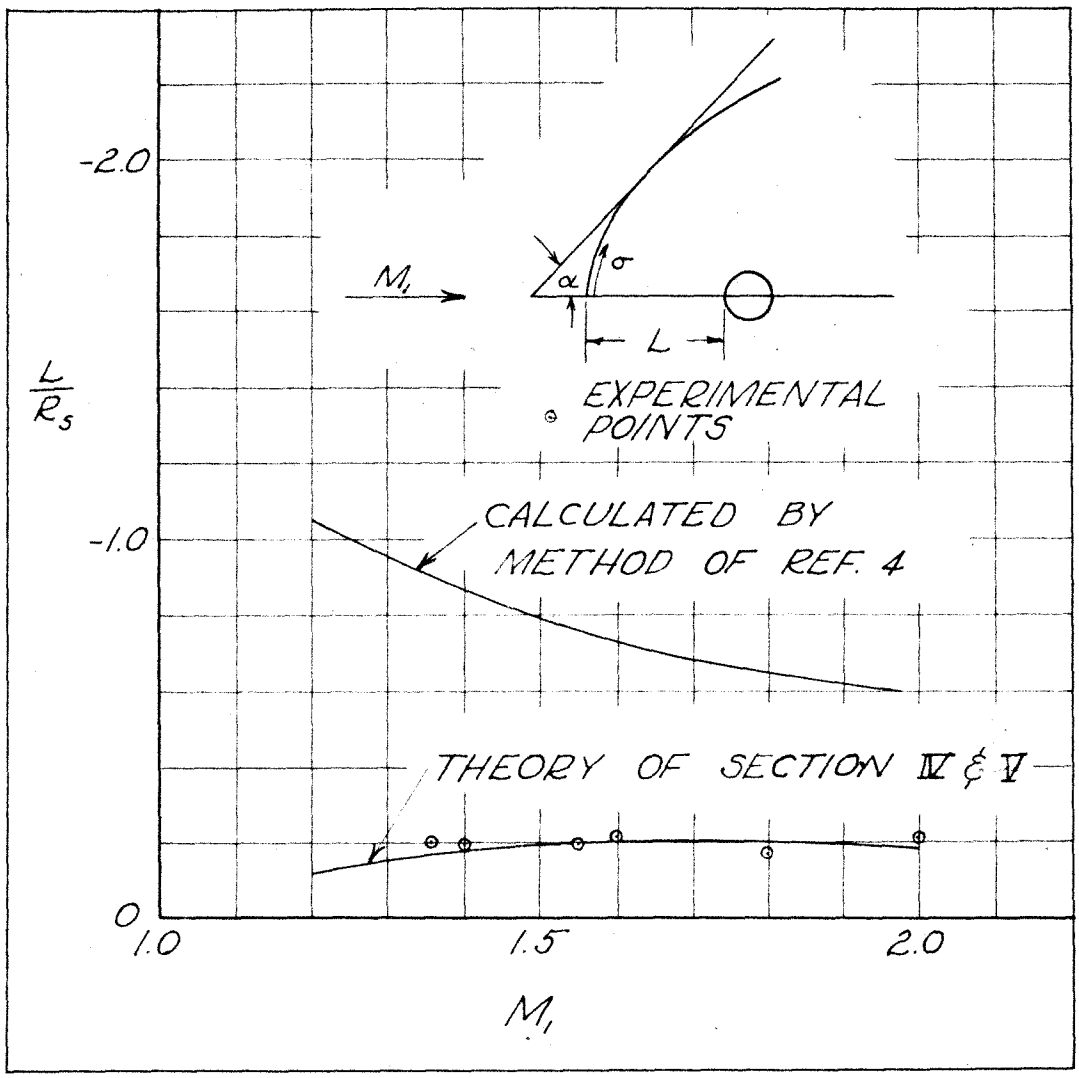

Fig. 14. Comparison of Theory (Ref. 4) with Experimental Data

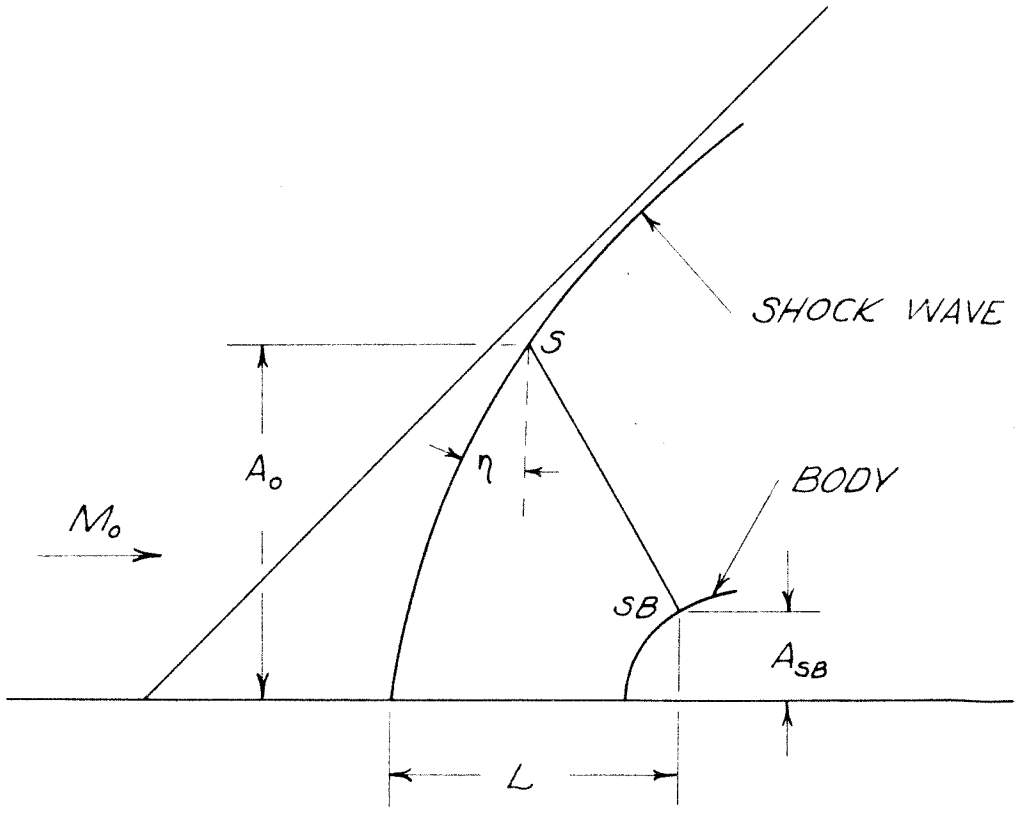

Fig. 15. Notation for Discussion of Moeckel's Theory

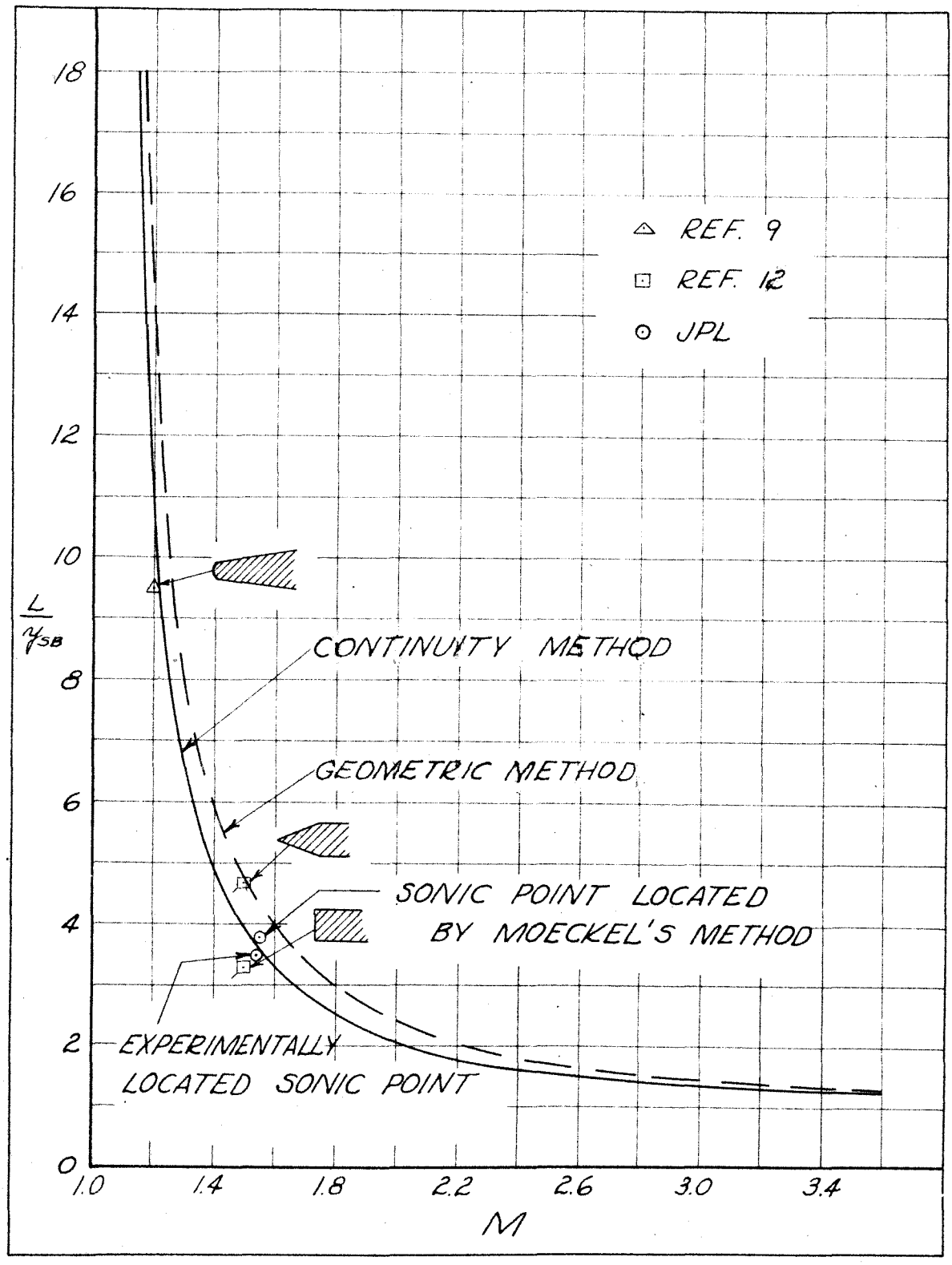

Fig. 16. Theoretical and Experimental Shock Location

Moeckel's Theory (Ref. 8)

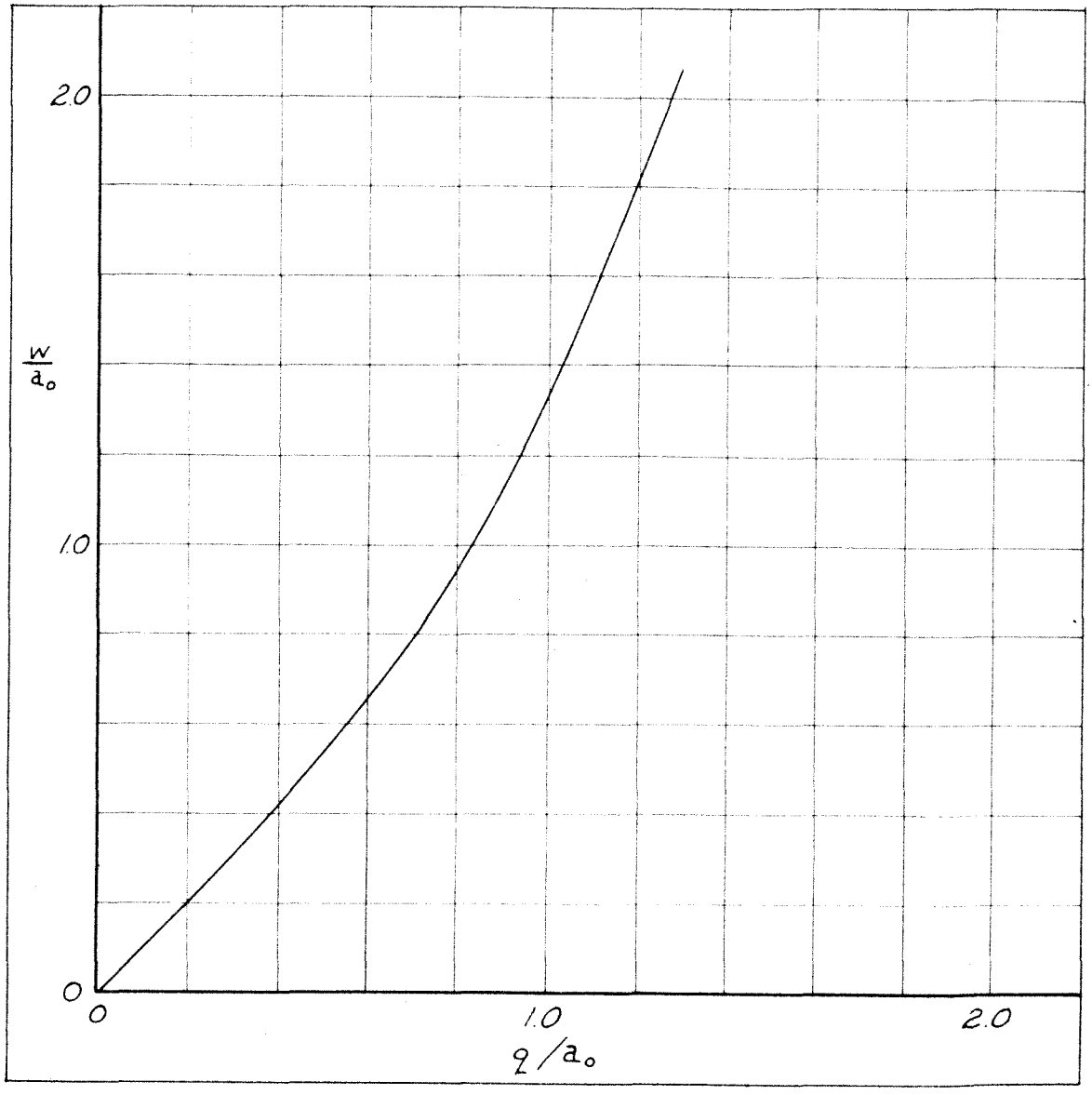

Fig. 17. Relationship Between Compressible and Incompressible Velocity

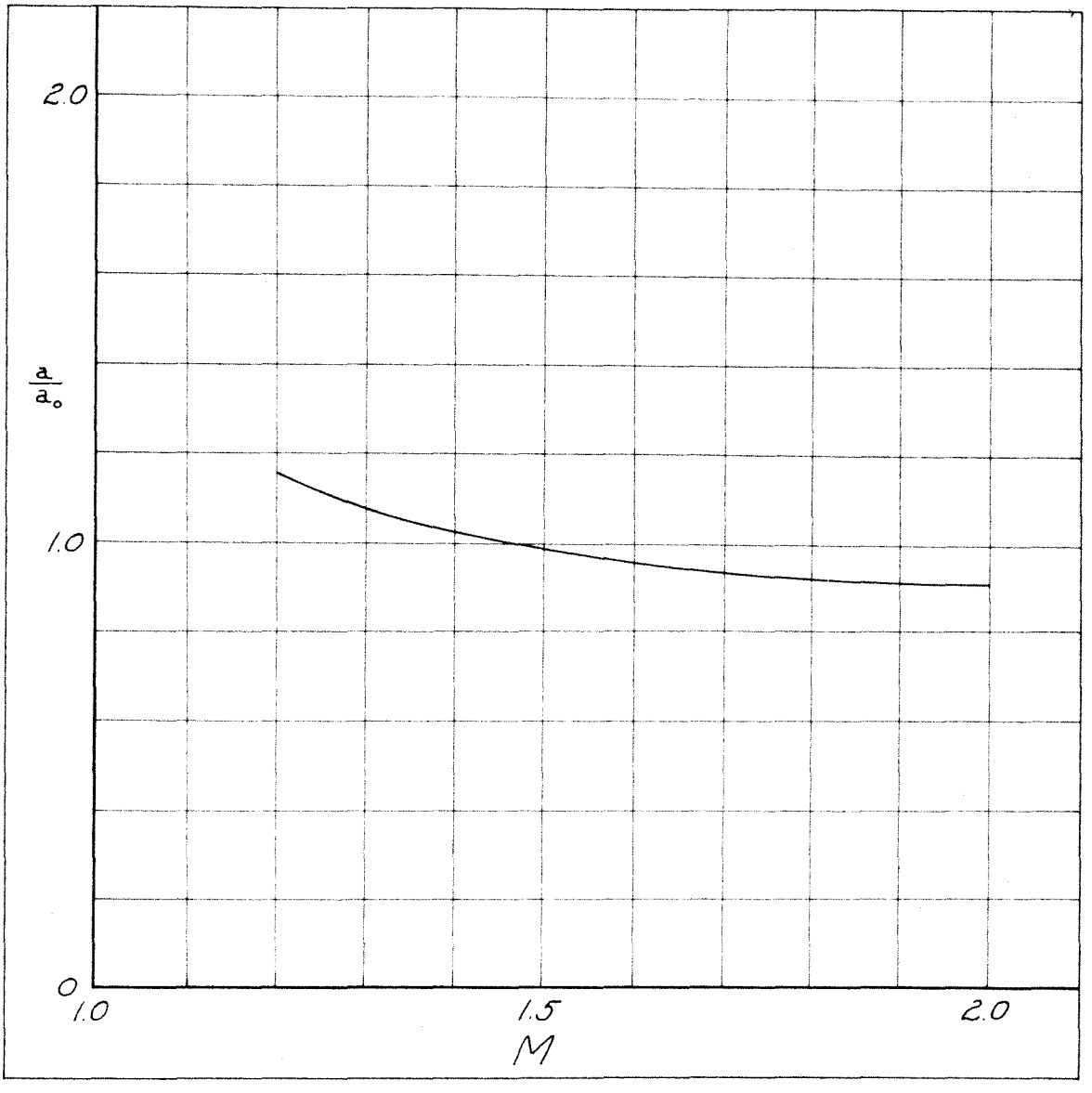

Fig. 1[illegible]. Velocity at Infinity in Incompressible Plane for Theory of Section V